Higher-order accurate two-step finite difference schemes for the many-dimensional wave equation

Higher-order Accurate Two-step Finite Difference Schemes for the Many-dimensional Wave Equation

Stefan Bilbao[a,*], Brian Hamilton[a]

[a] *Acoustics and Audio Group. James Clerk Maxwell Building, King's Buildings, University of Edinburgh, Edinburgh, UK, EH9 3JZ*

Abstract

The accurate simulation of wave propagation is a problem of longstanding interest. In this article, the focus is on higher-order accurate finite difference schemes for the wave equation in any number of spatial dimensions. In particular, two step schemes (which operate over three time levels) are studied. A novel approach to the construction of schemes exhibiting both isotropy and accuracy is presented using modified equation techniques, and allowing for the specification of precise stencils of operation for the scheme, and thus direct control over stencil size and thus operation counts per time-step. Both implicit and explicit schemes are presented, as well as parameterised families of such schemes under conditions specifying the order of isotropy and accuracy. Such conditions are framed in terms of a set of coupled constraints which are nonlinear in general, but linear for a fixed Courant number. Depending on the particular choice of stencils, it is often possible to develop schemes for which the traditional Courant-Friedrichs-Lewy condition is exceeded. A wide variety of families of such schemes is presented in one, two and three spatial dimensions, and accompanied by illustrations of numerical dispersion as well as convergence results confirming higher-order accuracy up to eighth order.

Keywords: wave equation, finite difference method, modified equations, higher-order accuracy

1. Introduction

The numerical simulation of wave propagation is an important application and object of study in itself for many fields, including electromagnetics, geophysics, and acoustics. In such fields, the linear wave equation in many spatial dimensions is often used as a basic test problem for the construction of numerical methods. Solutions to the wave equation can be approximated through various numerical techniques, such as finite difference [1, 2], finite element [3, 4], finite volume [5], and spectral methods [6]. Of these mentioned, the finite difference method is perhaps the oldest technique to be applied to numerically solve the wave equation, going back at least as far as the seminal work of Courant [7], and still constituting a popular choice for numerical discretisation today, particularly in geophysical [8] and CFD applications [9].

An important limitation of any numerical method for the many-dimensional wave equation that operates locally in space and/or time is erroneous numerical dispersion. Spectral methods, though in theory without error in the approximation of the spatial part of a problem, can be challenging to adapt to domains of non-trivial geometry, and, furthermore, remain susceptible to time discretisation error. For this reason, finite difference schemes are often preferred, but the problem of numerical dispersion [10, 11] requires grid resolution beyond the minimum two points per wavelength (on the regular Cartesian grid)— this quickly becomes infeasible in terms of computational cost for many-dimensional problems and/or large domains, despite the increasing availability of computing power and parallel hardware (such as Graphics Processing Units or GPUs) [12, 13]. On the other hand, high-order accurate schemes [14, 2] inherently have improved numerical dispersion in the limit of low wavenumbers. High-order methods can be seen as intermediate

*Corresponding author
Email address: sbilbao@staffmail.ed.ac.uk (Stefan Bilbao)

between low-order methods and spectral methods [15], and thus offer a flexible trade-off between the ability to impose boundary conditions and the ability to accurately resolve propagating wavefronts.

The standard approach to designing high-order accurate schemes for the wave equation—which, strictly speaking, requires that both time and space operators be approximated to high orders—is to employ conventional high-order spatial differences [16, 17], often over an equivalent first-order hyperbolic system, combined with high-order time integration (such as Runge-Kutta [18, 19, 20, 9]). Although these techniques have shown much success, there are gains in computational efficiency to be had by working with the second-order wave equation directly (as pointed out in, e.g., [21, 22, 23]). Rather than employing high-order time integrators, which necessarily require intermediate steps and possibly additional temporary states to be stored in memory (beyond the minimum of two for a second-order system), it is possible to achieve high-order accuracy, at least for the initial value problem, using only conventional two-step leapfrog (Störmer-Verlet [24]) integration, i.e., storing only the minimal two states in memory. The manner by which this is typically accomplished is known as the *modified equation approach* [25, 26, 27, 28, 29, 30, 31, 14, 32, 33, 34], wherein the scheme is expanded in a Taylor series such that temporal truncation errors can be recast in terms of spatial operators and then discretised. This leads to a delicate balancing of temporal and spatial truncation errors such that they effectively cancel up to a high order.

In this paper, a novel approach to modified equation methods is applied to finite difference schemes over regular Cartesian grids in order to achieve high even-order spatiotemporal accuracy for the homogeneous constant-coefficient wave equation in d spatial dimensions. Within this approach, general parametrised constructions for the d-dimensional Laplacian are combined with constraints imposed for high-order isotropy and accuracy. Constraints for isotropy are linear in the scheme coefficients, and constraints for higher-order accuracy are dependent on the Courant number. Thus such constraints may be viewed as linear if the Courant number is specified *a priori*, and nonlinear if the Courant number is treated as a partially free additional parameter, subject to a stability condition bounding it (normally from above), but still allowed to take on values over a continuous range. In either case, parameters of high-order accurate schemes, possibly dependent on the Courant number, are obtained as solutions to a resulting linear system. Even-order schemes to any order of accuracy have previously been derived for the many-dimensional wave equation using modified equation approaches, but they tend to produce minimal "diamond"-shaped stencils [30, 8] that are limited in terms of stability by the standard Courant-Friedrichs-Lewy condition. In contrast to such approaches and other applications of modified equations to leapfrog time-integrators [14, 22, 35], the general construction presented in this study offers more flexibility for choices of spatial discretisations that effectively cancel out temporal errors, allowing a wide variety of stencil shapes, along with the ability to impose additional high orders of isotropy (enabling, e.g., $2M$th-order accurate schemes with errors isotropic to $(2M+2)$th order, $M = 1, 2, \dots$). Schemes over diamond-shaped stencils are obtained as special cases. As shown in this paper, the resulting schemes can have Courant numbers close to unity, permitting larger time-steps for a fixed grid resolution than conventional diamond-shaped schemes [30, 8]. Additionally, this general construction permits implicit two-step time integration (e.g., *theta schemes* [34]), offering high-order accuracy with smaller spatial stencils than explicit counterparts (at the cost of sparse linear system solutions at each time-step). Throughout this work, many novel schemes are derived in one, two, and three spatial dimensions, and up to eighth-order accuracy. Stability conditions are obtained through frequency-domain analyses, and the reported orders of accuracy are confirmed through convergence analyses of numerical dispersion and via numerical simulations of wave propagation.

It should be mentioned that the scope of this paper lies with the initial value problem, and as such, boundary conditions beyond periodic ones will not be addressed in this work (as in, e.g., [8]), and are left to be developed in subsequent studies. Possible avenues to deal with non-periodic boundaries are discussed in Section 6.

A brief presentation of the many-dimensional wave equation appears in Section 2. In Section 3, basic time and space difference operations over regular Cartesian grids are presented, and in particular parametrised approximations to the Laplacian operator over arbitrary symmetric stencils, as well as conditions for higher-order isotropy. A general family of implicit and explicit two-step schemes for the many-dimensional wave equation appears in Section 4, accompanied by conditions for numerical stability and accuracy to higher order in space and time. Accuracy conditions may be expressed as a set of nonlinear constraints in the free parameters and the Courant number. In Section 5, various examples of higher-order accurate schemes in 1D, 2D and 3D are given, along with numerical results illustrating the rate of convergence. Conclusions

and final remarks are given in Section 6. Some additional material, with regard to various features of the designs presented here, appears in the Appendices. In Appendix A, energy-based approaches to the problem of numerical stability verification are presented, and in Appendix B, some conditions for negativity of parameterised approximations to the Laplacian are offered. Appendix C provides a brief link between the implicit family of schemes presented here and the familiar so-called theta family of schemes.

2. The Wave Equation

The wave equation in d spatial dimensions is defined as

$$\mathcal{L}u = 0\,, \qquad \text{where} \qquad \mathcal{L} = \partial_t^2 - \Delta\,. \tag{1}$$

Here, $u(\mathbf{x}, t)$ is the variable to be solved for as a function of time $t \in [0, \infty]$, and for coordinates $\mathbf{x} \in \mathcal{D} \subset \mathbb{R}^d$. ∂_t represents partial differentiation with respect to time, and Δ is the d-dimensional Laplacian operator, defined as

$$\Delta = \sum_{\nu=1}^{d} \partial_\nu^2\,, \tag{2}$$

where ∂_ν indicates partial differentiation with respect to spatial coordinate ν, for $\nu = 1, \ldots, d$. The problem has been nondimensionalized such that the wave speed is 1. In this study, it is assumed that $\mathcal{D} = \mathbb{R}^d$, and that there are no forcing terms, so that only the initial value problem is considered. The wave equation (1) must thus be complemented by two initial conditions:

$$u(\mathbf{x}, 0) = v_0(\mathbf{x}) \qquad \text{and} \quad \partial_t u(\mathbf{x}, t)|_{t=0} = v_1(\mathbf{x}) \tag{3}$$

for some functions $v_0(\mathbf{x})$ and $v_1(\mathbf{x})$ defined over $\mathbf{x} \in \mathbb{R}^d$.

2.1. Characteristic Equation

A monochromatic wavelike solution is of the form

$$u = e^{j\omega t + j\boldsymbol{\zeta}\cdot\mathbf{x}}\,, \tag{4}$$

where $\omega \in \mathbb{R}$ is an angular frequency, and $\boldsymbol{\zeta} \in \mathbb{R}^d$ is a d-dimensional wave vector ($|\boldsymbol{\zeta}|$ is the wavenumber and $2\pi/|\boldsymbol{\zeta}|$ is the wavelength). When inserted into the wave equation (1), a characteristic equation results:

$$P(\boldsymbol{\zeta}, \omega) = 0 \qquad \text{where} \qquad P(\boldsymbol{\zeta}, \omega) = -\omega^2 + |\boldsymbol{\zeta}|^2\,. \tag{5}$$

Here $P(\boldsymbol{\zeta}, \omega)$ is the Fourier symbol of $\mathcal{L}$. The solutions to (5) are the dispersion relations:

$$\omega = \pm|\boldsymbol{\zeta}|\,. \tag{6}$$

Taking the positive-valued solution above, the phase velocity, defined as $v_\phi = \omega/|\boldsymbol{\zeta}|$ is a constant equal to 1. The characteristic equation for the wave equation will be used in the analysis of modified equation methods for finite difference schemes in Section 4.2, and the resulting dispersion relation (6) will be employed for comparison against numerical results in Section 5.

3. Grid and Difference Approximations

Assume a grid function $u_{\mathbf{l}}^n$, defined over the uniform Cartesian grid $\mathbf{l} = [l_1 \ldots, l_d] \in \mathbb{Z}^d$ and for time steps $n \in \mathbb{Z}^+ = [0, 1, \ldots]$. Such a grid function represents an approximation to $u(\mathbf{x}, t)$ at locations $\mathbf{x} = \mathbf{l}h$, and at time instants $t = nk$, where h is the grid spacing, and k is the time step.

3.1. Time Shift and Difference Approximations

Time shift operators e_{t+} and e_{t-} may be defined, in terms of their action on the grid function $u_{\mathbf{l}}^n$ as

$$e_{t+}u_{\mathbf{l}}^n = u_{\mathbf{l}}^{n+1} \qquad e_{t-}u_{\mathbf{l}}^n = u_{\mathbf{l}}^{n-1}\,, \tag{7}$$

and the standard two-step approximation to the second time derivative may be written as

$$\delta_{tt} = \frac{1}{k^2}\left(e_{t+} - 2 + e_{t-}\right) = \partial_t^2 + O(k^2)\,. \tag{8}$$

In isolation, the operator δ_{tt} is formally second-order accurate. In certain analysis settings, it is appropriate to apply such operators to continuously variable functions; for example, the shift operator e_{t+}, when applied to a function $u(\mathbf{x}, t)$ would yield $e_{t+}u(\mathbf{x}, t) = u(\mathbf{x}, t + k)$. The use of shift and difference operators in this way should be clear from context.

3.2. Approximations to the Laplacian

There are many approaches to the approximation of the Laplacian operator over a Cartesian grid (e.g., [36, 30, 37, 38]). In this article, they will be constructed according to *shells* of grid locations located symmetrically about the point of application of the operator itself. A given shell is defined here in terms of an integer-valued vector $\mathbf{q}$—at a given grid point in a d-dimensional Cartesian grid, the shell of points associated with vector $\mathbf{q}$ is the set of grid points which are permutations of $\mathbf{q}$ grid spacings distant. Here a vector $\mathbf{q}$ is called *admissible* if $q_1, \ldots, q_d$ are non-negative, with $q_1 \geq 1$, and $q_m \leq q_{m-1}$ for $m = 2, \ldots, d$. The admissibility restriction above allows for unique association of any neighbouring grid point with a given shell.

A representation of a general Laplacian operator in terms of shells allows for a convenient parametrisation of general Laplacian approximations over non-overlapping stencils. Additionally, this allows for the association of a fixed operation count or computational cost with each shell, since the number of operations (and memory accesses) required per time-step is proportional to the stencil size.

It is useful to begin by defining basic spatial shift and averaging operations over a Cartesian grid. Spatial shift operators $e_{\nu\pm}$, $\nu = 1, \ldots, d$, may be defined as

$$e_{\nu+}u^n_{[l_1,\ldots,l_\nu,\ldots,l_d]} = u^n_{[l_1,\ldots,l_\nu+1,\ldots,l_d]} \qquad e_{\nu-}u^n_{[l_1,\ldots,l_\nu,\ldots,l_d]} = u^n_{[l_1,\ldots,l_\nu-1,\ldots,l_d]}\,. \tag{9}$$

Spatial averaging operators $\mu_\nu^{(b)}$, for $\nu = 1 \ldots, d$ and for $b = 0, 1, \ldots$ may be defined as

$$\mu_\nu^{(b)} = \frac{1}{2}\left(e_{\nu+}^b + e_{\nu-}^b\right) = 1 + \frac{b^2h^2}{2}\partial_\nu^2 + O(h^4)\,. \tag{10}$$

The bth power of the operator $e_{\nu\pm}$ is interpreted as a b-fold operator composition, and where $b = 0$ (the zeroth power) corresponds to the identity operation. The operator $\mu_\nu^{(b)}$ selects grid locations b steps away from the point of application in dimension ν.

A series of approximations $\delta_{\mathbf{q}}$ to the Laplacian operator, indexed by an integer-valued d-vector $\mathbf{q} = [q_1, \ldots, q_d]$, may be written as

$$\delta_{\mathbf{q}} = \frac{2}{(d-1)!h^2\|\mathbf{q}\|^2}\underbrace{\sum_{\boldsymbol{\gamma}\in\mathbb{P}(\mathbf{q})}\left(-1 + \prod_{j=1}^{d}\mu_j^{(\gamma_j)}\right)}_{\Xi_{\mathbf{q}}} = \Delta + O(h^2)\,. \tag{11}$$

The sum is over the vectors $\boldsymbol{\gamma} = [\gamma_1, \ldots, \gamma_d]$ which are the $d!$ permutations of the vector $\mathbf{q}$, indicated as $\mathbb{P}(\mathbf{q})$.

To examine the consistency of this operator with the Laplacian, consider the operator $\Xi_{\mathbf{q}}$ appearing in (11) above. Using (10), one may write:

$$\Xi_{\mathbf{q}} = \sum_{\boldsymbol{\gamma}\in\mathbb{P}(\mathbf{q})}\left(-1 + \prod_{j=1}^{d}\left(1 + \frac{\gamma_j^2h^2}{2}\partial_j^2 + O(h^4)\right)\right) \tag{12a}$$

$$= \frac{h^2}{2}\sum_{\boldsymbol{\gamma}\in\mathbb{P}(\mathbf{q})}\left(\sum_{j=1}^{d}\gamma_j^2\partial_j^2\right) + O(h^4) \tag{12b}$$

But, by symmetry over the sum of all permutations of $\mathbf{q}$,

$$\Xi_{\mathbf{q}} = \frac{(d-1)!h^2}{2}\left(\sum_{j=1}^{d} q_j^2\right)\left(\sum_{j=1}^{d} \partial_j^2\right) + O(h^4) = \frac{(d-1)!\|\mathbf{q}\|^2 h^2}{2}\Delta + O(h^4) \tag{13}$$

See Figure 1, illustrating the stencils of several such operators for $d = 1, 2, 3$. Notice that such stencils are not dense, motivating the use of the word "shell" used above to describe such stencils. The forms here are useful in the sense that, at least for explicit schemes, the operation count associated with such sparse-stencil operators is obvious from the stencil diagram. Indeed, for $d = 1$, each shell consists of three points; for $d = 2$ either four or eight; and for $d = 3$, any of six, eight, 12, 24 or 48 points.

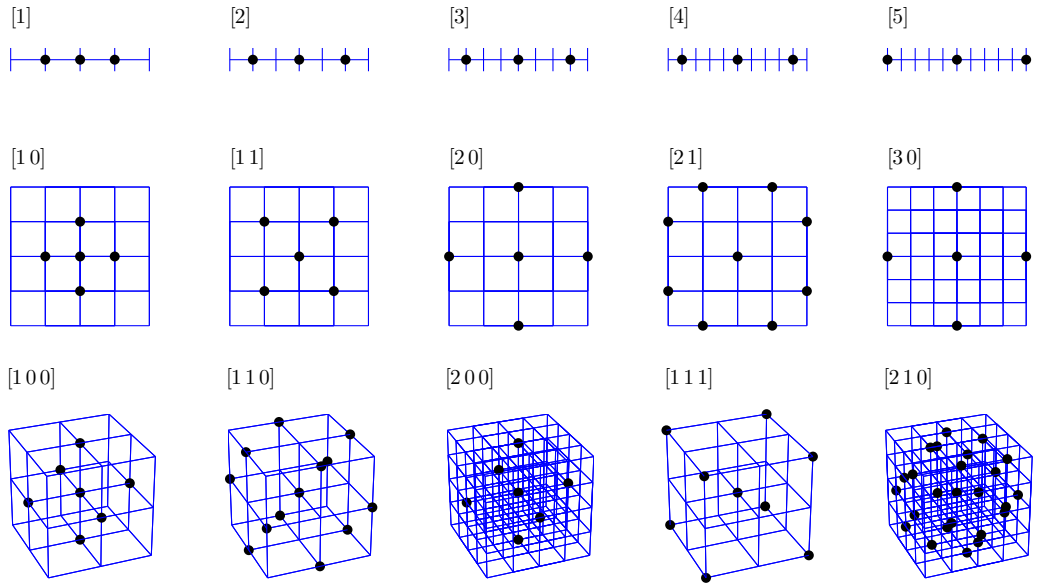

Figure 1: Stencils for the discrete Laplacian approximations $\delta_{\mathbf{q}}$, as defined in (11), for different choices of the index vector $\mathbf{q}$, as indicated. Stencils for $d = 1$ are shown in the top row, $d = 2$ in the second row, and for $d = 3$ in the bottom row.

3.3. Parameterized Approximations to the Laplacian

Consider now a set $\mathcal{Q} = \{\mathbf{q}_1, \ldots, \mathbf{q}_N\}$ of N distinct admissible d-vectors. A useful ordering of the vectors, which will be adopted here subsequently, is such that $\|\mathbf{q}_1\|_1 \leq \|\mathbf{q}_2\|_1 \leq \ldots \leq \|\mathbf{q}_N\|_1$, where $\|\cdot\|_1$ indicates the 1-norm of a vector. In cases for which two admissible vectors possess the same 1-norm, they are ordered lexicographically. A parameterized approximation to the Laplacian over $\mathcal{Q}$, to within a constant multiplicative factor, is then given by

$$\delta_{\mathcal{Q},\boldsymbol{\alpha}} = \sum_{p=1}^{N} \alpha_p \delta_{\mathbf{q}_p} = \left(\sum_{p=1}^{N} \alpha_p\right)\Delta + O(h^2) \tag{14}$$

in terms of the parameter vector $\boldsymbol{\alpha} = [\alpha_1, \ldots, \alpha_N]^{\mathrm{T}}$. Diagrams illustrating the stencils of such parameterised approximations, for $d = 1, 2, 3$ appear in Section 5.

From (11), such an approximation to the Laplacian is also second-order accurate in h (to within a constant multiplicative factor). However, if a constrained set $\boldsymbol{\alpha}$ of parameters is employed, i.e.,

$$\sum_{p=1}^{N} \alpha_p = 1\,, \tag{15}$$

then the multiplicative factor is unity, and $\hat{\delta}_{\mathcal{Q},\boldsymbol{\alpha}}$ (note the hat notation) is consistent with the Laplacian, and indeed approximates it to second-order accuracy in h:

$$\hat{\delta}_{\mathcal{Q},\boldsymbol{\alpha}} = \sum_{p=1}^{N} \alpha_p \delta_{\mathbf{q}_p} = \Delta + O(h^2)\,. \tag{16}$$

It is useful to have both constrained and unconstrained versions of the Laplacian operator—the constrained form given in (16) will be used, for consistency, when approximating the primary Laplacian appearing in (1). The unconstrained form will be used as an additional term in implicit designs, and will not need to be consistent with the Laplacian.

3.4. Operator Expansions

The difference operators defined in (8) and (11) are formally second-order accurate, in the time step k and grid spacing h respectively. In the interest of developing schemes of higher accuracy, it is useful to present full expansions of these operators in terms of their continuous counterparts.

The expansion for δ_{tt} may be written, in terms of powers of ∂_t, as

$$\delta_{tt} = \sum_{m=1}^{\infty} \frac{2k^{2m-2}}{(2m)!} \partial_t^{2m}\,. \tag{17}$$

The averaging operators $\mu_\nu^{(b)}$, in the spatial coordinate ν, can be expanded in terms of powers of ∂_ν as

$$\mu_\nu^{(b)} = \sum_{\eta=0}^{\infty} \frac{h^{2\eta} b^{2\eta}}{(2\eta)!} \partial_\nu^{2\eta}\,. \tag{18}$$

Returning now to the expression for a Laplacian approximation $\delta_{\mathbf{q}}$ defined over a shell of index $\mathbf{q}$, from (11), and examining again the expression $\Xi_{\mathbf{q}}$, using (18), gives

$$\Xi_{\mathbf{q}} = \sum_{\boldsymbol{\gamma}\in\mathbb{P}(\mathbf{q})} \left(-1 + \prod_{j=1}^{d} \left(\sum_{\eta_j=0}^{\infty} \frac{h^{2\eta_j} \gamma_j^{2\eta_j}}{(2\eta_j)!} \partial_j^{2\eta_j} \right) \right)\,. \tag{19}$$

At this point, terms in the expansion of equal order of differentiation may be grouped. To this end, define the non-negative integer-valued vector $\boldsymbol{\eta} = [\eta_1, \ldots, \eta_d]$, and the set $\mathbb{M}^{(m)}$ by

$$\mathbb{M}^{(m)} = \{\boldsymbol{\eta} | \sum_{j=1}^{d} \eta_j = m\}\,. \tag{20}$$

$\Xi_{\mathbf{q}}$ may now be rewritten as

$$\begin{aligned} \Xi_{\mathbf{q}} &= \sum_{\boldsymbol{\gamma}\in\mathbb{P}(\mathbf{q})} \sum_{m=1}^{\infty} h^{2m} \sum_{\boldsymbol{\eta}\in\mathbb{M}^{(m)}} \prod_{j=1}^{d} \frac{\gamma_j^{2\eta_j}}{(2\eta_j)!} \partial_j^{2\eta_j} && (21) \\ &= \sum_{m=1}^{\infty} h^{2m} \sum_{\boldsymbol{\eta}\in\mathbb{M}^{(m)}} \left(\prod_{j=1}^{d} \partial_j^{2\eta_j} \right) \left(\sum_{\boldsymbol{\gamma}\in\mathbb{P}(\mathbf{q})} \prod_{j=1}^{d} \frac{\gamma_j^{2\eta_j}}{(2\eta_j)!} \right)\,. && (22) \end{aligned}$$

Now, define the coefficients $g_{\mathbf{q}}^{(\boldsymbol{\eta})}$ and $\epsilon_{\mathbf{q}}^{(m)}$ as

$$g_{\mathbf{q}}^{(\boldsymbol{\eta})} = \frac{1}{(d-1)!\|\mathbf{q}\|_{2m}^{2m}} \frac{(2m)!}{(2\boldsymbol{\eta})!} \sum_{\boldsymbol{\gamma}\in\mathbb{P}(\mathbf{q})} \prod_{j=1}^{d} \gamma_j^{2\eta_j} \qquad \epsilon_{\mathbf{q}}^{(m)} = \frac{\|\mathbf{q}\|_{2m}^{2m}}{\|\mathbf{q}\|_2^2}\,, \tag{23}$$

where $\|\mathbf{q}\|_{2m}$ indicates the $2m$-norm of the vector $\mathbf{q}$. Here, multi-index notation has been used, i.e., $(2\boldsymbol{\eta})! = (2\eta_1)!(2\eta_2)!\ldots(2\eta_d)!$. The resulting expression for $\Xi_{\mathbf{q}}$ is then

$$\Xi_{\mathbf{q}} = (d-1)!\|\mathbf{q}\|_2^2 \sum_{m=1}^{\infty} \frac{h^{2m}\epsilon_{\mathbf{q}}^{(m)}}{(2m)!} \sum_{\boldsymbol{\eta}\in\mathbb{M}^{(m)}} g_{\mathbf{q}}^{(\boldsymbol{\eta})} \prod_{j=1}^{d} \partial_j^{2\eta_j}\,, \tag{24}$$

and, finally, for $\delta_{\mathbf{q}}$ as

$$\delta_{\mathbf{q}} = \sum_{m=1}^{\infty} \frac{2h^{2m-2}\epsilon_{\mathbf{q}}^{(m)}}{(2m)!} \sum_{\boldsymbol{\eta}\in\mathbb{M}^{(m)}} g_{\mathbf{q}}^{(\boldsymbol{\eta})} \prod_{j=1}^{d} \partial_j^{2\eta_j}\,. \tag{25}$$

It is also of interest to examine powers of the Laplacian operator Δ, which may be written, in terms of powers of the constituent operators ∂_ν, $\nu = 1,\ldots,d$, using the multinomial expansion, as

$$\Delta^m = \left(\sum_{j=1}^{d} \partial_j^2\right)^m = \sum_{\boldsymbol{\eta}\in\mathbb{M}^{(m)}} f^{(\boldsymbol{\eta})} \prod_{j=1}^{d} \partial_j^{2\eta_j} \qquad \text{where} \qquad f^{(\boldsymbol{\eta})} = \frac{m!}{\boldsymbol{\eta}!}\,. \tag{26}$$

3.5. Coefficient Symmetries

For a given order $m \geq 1$, the coefficients $f^{(\boldsymbol{\eta})}$ and $g_{\mathbf{q}}^{(\boldsymbol{\eta})}$ are defined for $\boldsymbol{\eta} \in \mathbb{M}^{(m)}$. These sets of coefficients possess certain symmetries, which follow from the symmetry of the Laplacian Δ and the approximations $\delta_{\mathbf{q}}$ with respect to the individual coordinates. It is thus useful, before imposing any constraints on these coefficients (for isotropy and accuracy), to eliminate redundancy in the set of coefficients.

First, note that these coefficients are unchanged under any permutation $\mathbb{P}(\boldsymbol{\eta})$ of $\boldsymbol{\eta}$. Furthermore, note that for the d distinct permutations of the vector $[m,0,\ldots,0]$, $\mathbb{P}([m,0,\ldots,0])$, $f^{(\boldsymbol{\eta})} = 1$ and $g_{\mathbf{q}}^{(\boldsymbol{\eta})} = 1$. These observations suggest that one need only consider vectors $\boldsymbol{\eta}$ within the reduced set

$$\tilde{\mathbb{M}}^{(m)} = \{\boldsymbol{\eta} \in \mathbb{M}^{(m)} | \eta_1 \geq \eta_2 \geq \ldots \geq \eta_d, \eta_2 \neq 0\}\,. \tag{27}$$

The reduced set $\tilde{\mathbb{M}}^{(m)}$ can be viewed as indexing the distinct mixed-derivative terms in the operator expansion as a whole. Also, for any admissible $\mathbf{q} = [q_1,\ldots,q_d]$ with $q_2 = \ldots = q_d = 0$, $g_{\mathbf{q}}^{(\boldsymbol{\eta})} = 0$, for $\boldsymbol{\eta} \in \tilde{\mathbb{M}}^{(m)}$. In other words, the expansion for the discrete Laplacian under such a choice of $\mathbf{q}$, for which the stencil includes only points directly on the grid axes relative to the point of application of the operator does not possess any mixed-derivative terms. Such is the case for all members of the "star-shaped" families of approximations to the Laplacian (such as in, e.g., conventional high-order approximations to the Laplacian [17]). See Section 5.2.3.

3.6. Isotropy

The following is a derivation of linear constraints to impose for isotropy up to a given order in the discrete Laplacian. Isotropy is generally a desirable property in discrete Laplacians [36, 37, 39, 38] for PDE problems involving the Laplacian operator, which itself is an isotropic operator. High-order isotropy can be used for post-processing of dispersion errors [40, 41]. For this study, the main motivation for deriving high-order isotropy is that it is a necessary step in acheiving high-order accuracy in two-step schemes through modified equation methods.

Consider the parameterized operators of the form $\delta_{\mathcal{Q},\boldsymbol{\alpha}}$ as given in (14), for an arbitrary set of admissible index vectors $\mathcal{Q} = \{\mathbf{q}_1,\ldots,\mathbf{q}_N\}$. Using the operator expansion (25), it may be rewritten as

$$\delta_{\mathcal{Q},\boldsymbol{\alpha}} = \sum_{m=1}^{\infty} \frac{2h^{2m-2}}{(2m)!} \sum_{p=1}^{N} \alpha_p \epsilon_{\mathbf{q}_p}^{(m)} \sum_{\boldsymbol{\eta}\in\mathbb{M}^{(m)}} g_{\mathbf{q}_p}^{(\boldsymbol{\eta})} \prod_{j=1}^{d} \partial_j^{2\eta_j}\,. \tag{28}$$

Matching the M first terms between the expansion (28) and the expansion (26) for powers of the Laplacian operators, then the constraints

$$\sum_{p=1}^{N} \alpha_p \epsilon_{\mathbf{q}_p}^{(m)} \left(g_{\mathbf{q}_p}^{(\boldsymbol{\eta})} - f^{(\boldsymbol{\eta})}\right) = 0, \qquad \boldsymbol{\eta} \in \tilde{\mathbb{M}}^{(m)} \qquad \text{for} \qquad m = 1,\ldots,M \tag{29}$$

lead to the following simplification for the operator expansion, which can now be written in terms of powers of the Laplacian Δ up to the Mth power, as

$$\delta^{(M)}_{\mathcal{Q},\boldsymbol{\alpha}} = \sum_{m=1}^{M} \frac{2h^{2m-2}}{(2m)!} r^{(m)}_{\mathcal{Q},\boldsymbol{\alpha}} \Delta^m + O(h^{2M}) \qquad \text{where} \qquad r^{(m)}_{\mathcal{Q},\boldsymbol{\alpha}} = \sum_{p=1}^{N} \alpha_p \epsilon^{(m)}_{\mathbf{q}_p} \,. \tag{30}$$

The operator is thus isotropic to $2M$th order, as indicated by the superscript (M) in the expression for the parameterized operator in (30). Note, however, that the number of free parameters N characterising the Laplacian approximation must be sufficient to satisfy all the constraints given in (29). In order to achieve such isotropy for an operator, the number N of Laplacians in $\mathcal{Q}$ must generally be chosen as

$$N \geq N^{(M)} = \sum_{m=1}^{M} M^{(m)} \qquad \text{where} \qquad M^{(m)} = |\tilde{\mathbb{M}}^{(m)}| \,. \tag{31}$$

where $|\tilde{\mathbb{M}}^{(m)}|$ denotes the number of elements in $\tilde{\mathbb{M}}^{(m)}$. Note that $r^{(1)}_{\mathcal{Q},\boldsymbol{\alpha}} = \sum_{p=1}^{N} \alpha_p$; if the operator is normalized such that (15) holds, then $r^{(1)}_{\mathcal{Q},\boldsymbol{\alpha}} = 1$.

The conditions above for isotropy are distinct from conditions for accuracy. From the expansion (28), conditions for accuracy of the Laplacian approximation to $2M$th order are

$$\sum_{p=1}^{N} \alpha_p \epsilon^{(m)}_{\mathbf{q}_p} g_{\mathbf{q}_p}{}^{(\boldsymbol{\eta})} = 0, \qquad \boldsymbol{\eta} \in \tilde{\mathbb{M}}^{(m)} \,, \tag{32}$$

and thus

$$\delta^{(M)}_{\mathcal{Q},\boldsymbol{\alpha}} = \Delta + O(h^{2M}) \,. \tag{33}$$

Such conditions also trivially imply isotropy to $2M$th order. While useful for time-independent problems, in the context of modified equation methods, such approximations are less so, as the powers of the Laplacian in the isotropic approximation may be cancelled with terms resulting from time discretisation, as will be discussed in Section 4.

3.7. Frequency Domain Representation

As a prelude to stability analysis in Section 4.2, it is useful to introduce the frequency domain representations of the various operators defined in the previous sections.

Considering again a monochromatic wavelike component, or ansatz, now defined over the grid as

$$u^n_{\mathbf{l}} = e^{j\omega nk + j\boldsymbol{\zeta}\cdot\mathbf{l}h} \tag{34}$$

for angular frequency ω and wave vector $\boldsymbol{\zeta} = [\zeta_1, \ldots, \zeta_d]$. ω and the various difference operators behave as multiplicative factors, which are periodic in ω and $\boldsymbol{\zeta}$. By multi-dimensional sampling considerations [42], the definitions of all such factors may be limited to the domains $\omega \in [-\pi/k, \pi/k]$ and the cube $\boldsymbol{\zeta} \in \mathbb{U}^d$, for $\mathbb{U}^d = [-\pi/h, \pi/h]^d$.

For the time difference operator δ_{tt} defined in (8), one has for solutions of the form (34):

$$\delta_{tt} u^n_{\mathbf{l}} = -\frac{4}{k^2} \sin^2\left(\frac{\omega k}{2}\right) u^n_{\mathbf{l}} \,, \tag{35}$$

and for convenience, the above relation is rewritten as:

$$\delta_{tt} \longrightarrow -\frac{4}{k^2} \sin^2\left(\frac{\omega k}{2}\right) . \tag{36}$$

For the averaging operators $\mu^{(b)}_{\nu}$, as defined in (10), one has:

$$\mu^{(b)}_{\nu} \longrightarrow c^{(b)}_{\nu}(\boldsymbol{\zeta}) \triangleq \cos(bk_\nu h) \qquad \nu = 1, \ldots, d \,, \tag{37}$$

and for the approximation $\delta_{\mathbf{q}}$ to the Laplacian defined in (11), one has:

$$\delta_{\mathbf{q}} \longrightarrow \frac{1}{h^2} D_{\mathbf{q}}(\boldsymbol{\zeta}) \qquad \text{where} \qquad D_{\mathbf{q}}(\boldsymbol{\zeta}) \triangleq \frac{2}{(d-1)!\|\mathbf{q}\|^2} \sum_{\boldsymbol{\gamma} \in \mathbb{P}(\mathbf{q})} \left(-1 + \prod_{j=1}^{d} c_j^{(\gamma_j)} \right) . \tag{38}$$

For a parametrised approximations to the Laplacian, defined over the index set $\mathcal{Q}$, and with coefficients $\boldsymbol{\alpha}$,

$$\delta_{\mathcal{Q},\boldsymbol{\alpha}} \longrightarrow D_{\mathcal{Q},\boldsymbol{\alpha}}(\boldsymbol{\zeta}) = \sum_{p=1}^{N} \alpha_p D_{\mathbf{q}_p}(\boldsymbol{\zeta}) . \tag{39}$$

4. A General Family of Two Step Schemes

Consider now a general family of two-step schemes for the d-dimensional wave equation which may be written, in operator form, as

$$\mathfrak{l} u_{\mathbf{l}}^n = 0 \qquad \text{where} \qquad \mathfrak{l} = \left(1 + h^2 \delta_{\mathcal{Q}^{(i)},\boldsymbol{\alpha}^{(i)}}\right) \delta_{tt} - \hat{\delta}_{\mathcal{Q}^{(e)},\boldsymbol{\alpha}^{(e)}} . \tag{40}$$

Two distinct approximations to the Laplacian appear, over (in general different) index sets $\mathcal{Q}^{(i)}$ and $\mathcal{Q}^{(e)}$, with associated parameter sets $\boldsymbol{\alpha}^{(i)}$ and $\boldsymbol{\alpha}^{(e)}$. Note that the operator $\hat{\delta}_{\mathcal{Q}^{(e)},\boldsymbol{\alpha}^{(e)}}$ is normalized, so that the parameter vector $\boldsymbol{\alpha}^{(e)}$ satisfies (15). The operator $\delta_{\mathcal{Q}^{(i)},\boldsymbol{\alpha}^{(e)}}$ is not normalized, and thus approximates the Laplacian to within a multiplicative constant. The scheme is consistent with the d-dimensional wave equation and, nominally, second-order accurate in the time step and grid spacing:

$$\mathfrak{l} = \mathcal{L} + O(h^2) + O(k^2) \tag{41}$$

where $\mathcal{L}$ is the operator corresponding to the wave equation, as defined in (1). If, additionally, the parameter set $\boldsymbol{\alpha}^{(i)}$ is identically zero, the scheme is explicit; otherwise, it is implicit. In either case, the scheme operates over three adjacent time levels, which is sometimes referred to as a two-step scheme. For the wave equation, which is second-order in time, it is minimal in terms of the number of time steps employed in a given update, and thus in terms of the resulting computer memory requirements. Simplifications that lead to previously derived schemes (e.g., [30, 14, 8]) will be discussed in Section 5.2.1. A simplification to obtain *theta schemes*, which can be seen as a subset of this general family using only one discrete Laplacian (rather than two), is shown in Appendix C.

In finite difference schemes for the wave equation, a particular parameter of great importance is the Courant number, defined as

$$\lambda = k/h . \tag{42}$$

In studies of accuracy and convergence of schemes for the wave equation, it is customary to hold λ constant as the time step (or grid spacing) is decreased. In this case, the accuracy of the scheme can be written either in terms of the grid spacing h or the time step k, as these are related by a constant, so

$$\mathfrak{l} = \mathcal{L} + O(h^2) = \mathcal{L} + O(k^2) . \tag{43}$$

Note that under the assumption of a constant Courant number, in schemes for which the order of accuracy is distinct in the grid spacing or time step, the order of accuracy collapses to that of the larger error term.

4.1. Accuracy to Higher Order

Assume first that the Laplacian approximation $\hat{\delta}_{\mathcal{Q}^{(e)},\boldsymbol{\alpha}^{(e)}}$ is isotropic to $2M$th order, for some $M \geq 1$, and the approximation $\delta_{\mathcal{Q}^{(i)},\boldsymbol{\alpha}^{(i)}}$ is isotropic to $2M^{(i)}$th order, for some $M^{(i)} \geq 1$. Using the operator expansions and accompanying definitions of the coefficients r in (30) leads to:

$$\hat{\delta}^{(M)}_{\mathcal{Q}^{(e)},\boldsymbol{\alpha}^{(e)}} = \sum_{m=1}^{M} \frac{2h^{2m-2}}{(2m)!} r^{(m)}_{\mathcal{Q}^{(e)},\boldsymbol{\alpha}^{(e)}} \Delta^m + O(h^{2M}) \tag{44a}$$

$$\delta^{(M^{(i)})}_{\mathcal{Q}^{(i)},\boldsymbol{\alpha}^{(i)}} = \sum_{m=1}^{M^{(i)}} \frac{2h^{2m-2}}{(2m)!} r^{(m)}_{\mathcal{Q}^{(i)},\boldsymbol{\alpha}^{(i)}} \Delta^m + O(h^{2M^{(i)}}) . \tag{44b}$$

Using the definition of the Courant number from (42), one may set $h = k/\lambda$, and, furthermore, using the fact that $r^{(1)}_{\mathcal{Q}^{(e)},\boldsymbol{\alpha}^{(e)}} = 1$ (in other words, the Laplacian approximation $\hat{\delta}^{(M)}_{\mathcal{Q}^{(e)},\boldsymbol{\alpha}^{(e)}}$ is normalized and consistent with the Laplacian), one may write

$$\begin{aligned}\hat{\delta}^{(M)}_{\mathcal{Q}^{(e)},\boldsymbol{\alpha}^{(e)}} &= \Delta + \sum_{m=2}^{M} \frac{2k^{2m-2}}{\lambda^{2m-2}(2m)!} r^{(m)}_{\mathcal{Q}^{(e)},\boldsymbol{\alpha}^{(e)}} \Delta^m + O(k^{2M}) \\ \delta^{(M^{(i)})}_{\mathcal{Q}^{(i)},\boldsymbol{\alpha}^{(i)}} &= \sum_{m=1}^{M^{(i)}} \frac{2k^{2m-2}}{\lambda^{2m-2}(2m)!} r^{(m)}_{\mathcal{Q}^{(i)},\boldsymbol{\alpha}^{(i)}} \Delta^m + O(k^{2M^{(i)}})\,.\end{aligned}$$

and, in addition, for the operator δ_{tt}, from (17)

$$\delta_{tt} = \partial_t^2 + \sum_{m=2}^{M} \frac{2k^{2m-2}}{(2m)!} \partial_t^{2m} + O(k^{2M})\,.$$

The discrete operator $\mathfrak{l}$ can now be expanded in ascending powers of the time step k, using the expansions (46) and (45), and . Provided that $M^{(i)} \geq M-1$, one then has:

$$\mathfrak{l} = \mathcal{L} + \sum_{m=2}^{M} \frac{2k^{2m-2}}{(2m)!} \mathfrak{l}^{(m)} + O(k^{2M})\,, \tag{46}$$

where

$$\mathfrak{l}^{(m)} = \partial_t^{2m} - \frac{r^{(m)}_{\mathcal{Q}^{(e)},\boldsymbol{\alpha}^{(e)}}}{\lambda^{2m-2}} \Delta^m + \sum_{\xi=1}^{m-1} \frac{w^{(m)}_{\xi} r^{(\xi)}_{\mathcal{Q}^{(i)},\boldsymbol{\alpha}^{(i)}}}{\lambda^{2\xi}} \Delta^{\xi} \partial_t^{2(m-\xi)} \qquad \text{for} \qquad m = 2, \ldots, M \tag{47}$$

with

$$w^{(m)}_{\xi} = \frac{2\,(2m)!}{(2\xi)!\,(2m-2\xi)!}\,. \tag{48}$$

The operator $\mathfrak{l}^{(m)}$ is a homogeneous bivariate polynomial equation of degree m in the operators ∂_t^2 and Δ; the central idea behind the modified equation method as applied here is to extract a factor of $\mathcal{L}$, the operator corresponding to the wave equation, as defined in (1). Writing, for the moment, $x = \partial_t^2$ and $y = \Delta$, then

$$\mathfrak{l}^{(m)}(x,y) = \sum_{p=0}^{m} b_p x^p y^{m-p} = 0$$

for some coefficients b_p, $p = 0 \ldots, m$. If $\mathcal{L} = \partial_t^2 - \Delta = x - y$ is a factor of $\mathfrak{l}^{(m)}(x,y)$, then

$$\mathfrak{l}^{(m)}(x,x) = 0 \qquad \Rightarrow \qquad \sum_{p=0}^{m} b_p x^m = 0 \qquad \Rightarrow \qquad \sum_{p=0}^{m} b_p = 0\,.$$

The converse holds as well. Thus, under the condition that the coefficients of $\mathfrak{l}^{(m)}$ sum to zero, or that

$$1 - \frac{r^{(m)}_{\mathcal{Q}^{(e)},\boldsymbol{\alpha}^{(e)}}}{\lambda^{2m-2}} + \sum_{\xi=1}^{m-1} \frac{w^{(m)}_{\xi} r^{(\xi)}_{\mathcal{Q}^{(i)},\boldsymbol{\alpha}^{(i)}}}{\lambda^{2\xi}} = 0 \qquad \text{for} \qquad m = 2, \ldots, M\,, \tag{49}$$

then $\mathfrak{l}^{(m)}$ can be factored as $\mathfrak{l}^{(m)} = \mathcal{L} \cdot \mathfrak{l}^{(m-1)}_{\text{rem}}$, for a homogeneous bivariate polynomial $\mathfrak{l}^{(m-1)}_{\text{rem}}$ of degree $m-1$. Thus, under the constraints (49), the operator $\mathfrak{l}$ may be written as

$$\mathfrak{l} = \mathcal{L}\left(1 + O(k^2)\right) + O(k^{2M})\,. \tag{50}$$

Finally, the scheme $\mathfrak{l}u = 0$ may then be written as

$$\left(1 + O(k^2)\right)\mathcal{L}u = O(k^{2M}) \qquad \text{or} \qquad \mathcal{L}u = O(k^{2M})\,, \tag{51}$$

and is thus accurate to order $2M$ in the time step (or grid spacing). This is the "modified equation" representation of the scheme (40), and the explicit constraint for $2M$th-order accuracy is given in (49).

Alternatively, one can arrive at constraints (49) by considering an *exact* solution u to the wave equation under the action of $\mathfrak{l}$. With an exact solution, one can use the relation: $\partial_t^{2m} = \Delta^m$ (following, e.g., [30, 14]) in order to replace powers of the Laplacian by temporal derivatives in (46) and (47). Then it is straightforward to see that the conditions (49) result in:

$$\mathfrak{l} = \mathcal{L} + O(k^{2M}) \,, \tag{52}$$

or accuracy to order $2M$ for the scheme.

4.2. Characteristic Equation and Stability

Using the frequency domain ansatz (34) from Section 3.7, the characteristic equation for the scheme (40) may be written as

$$\mathfrak{p}\left(\boldsymbol{\zeta}, \omega\right) u = 0 \qquad \text{where} \qquad \mathfrak{p}\left(\boldsymbol{\zeta}, \omega\right) = \left(1 + D_{\mathcal{Q}^{(i)}, \boldsymbol{\alpha}^{(i)}}\left(\boldsymbol{\zeta}\right)\right) \left(\frac{-4}{k^2} \sin^2\left(\frac{\omega k}{2}\right)\right) - \frac{1}{h^2} \hat{D}_{\mathcal{Q}^{(e)}, \boldsymbol{\alpha}^{(e)}}\left(\boldsymbol{\zeta}\right) \,, \tag{53}$$

and the solutions are given by

$$\sin^2\left(\frac{\omega k}{2}\right) = -\frac{\lambda^2}{4} \frac{\hat{D}_{\mathcal{Q}^{(e)}, \boldsymbol{\alpha}^{(e)}}\left(\boldsymbol{\zeta}\right)}{1 + D_{\mathcal{Q}^{(i)}, \boldsymbol{\alpha}^{(i)}}\left(\boldsymbol{\zeta}\right)} \,. \tag{54}$$

For oscillatory solutions, one must have $0 \leq \sin^2\left(\frac{\omega k}{2}\right) \leq 1$, for all wavenumbers $\boldsymbol{\zeta} \in \mathbb{U}^d$. This leads to two constraints on the parameter set $\left(\boldsymbol{\alpha}^{(e)}, \boldsymbol{\alpha}^{(i)}, \lambda\right)$:

$$\theta^{(e)}\left(\boldsymbol{\alpha}^{(e)}\right) = \min_{\boldsymbol{\zeta} \in \mathbb{U}^d} \left(-\hat{D}_{\mathcal{Q}^{(e)}, \boldsymbol{\alpha}^{(e)}}\left(\boldsymbol{\zeta}\right)\right) \quad \geq \quad 0 \,, \tag{55a}$$

$$\theta^{(C)}\left(\boldsymbol{\alpha}^{(e)}, \boldsymbol{\alpha}^{(i)}, \lambda\right) = \min_{\boldsymbol{\zeta} \in \mathbb{U}^d} \left(-\lambda^2 - \frac{4\left(1 + D_{\mathcal{Q}^{(i)}, \boldsymbol{\alpha}^{(i)}}\left(\boldsymbol{\zeta}\right)\right)}{\hat{D}_{\mathcal{Q}^{(e)}, \boldsymbol{\alpha}^{(e)}}\left(\boldsymbol{\zeta}\right)}\right) \quad \geq \quad 0 \,. \tag{55b}$$

The first condition is an inequality constraint over the coefficients for the explicit Laplacian operator. The second is an inequality constraint relating the explicit and implicit Laplacian coefficients and λ. It is important to point out that under constraints for higher-order accuracy, as given in (49), the coefficient sets $\boldsymbol{\alpha}^{(e)}$ and $\boldsymbol{\alpha}^{(i)}$ will themselves be dependent on the Courant number λ, and thus the constraints are not independent.

If higher-order accuracy constraints are not employed (but where constraints for isotropy may be), the second condition may be written in a more familiar form as

$$\lambda \leq \lambda_{\max}\left(\boldsymbol{\alpha}^{(e)}, \boldsymbol{\alpha}^{(i)}\right) = 2\sqrt{\min_{\boldsymbol{\zeta} \in \mathbb{U}^d} \left(-\frac{\left(1 + D_{\mathcal{Q}^{(i)}, \boldsymbol{\alpha}^{(i)}}\left(\boldsymbol{\zeta}\right)\right)}{\hat{D}_{\mathcal{Q}^{(e)}, \boldsymbol{\alpha}^{(e)}}\left(\boldsymbol{\zeta}\right)}\right)} \,, \tag{56}$$

which can be interpreted as a direct bound on the Courant number λ in terms of the coefficient sets, as is commonly the case in finite difference schemes.

None of the constraints is of a particularly smooth form; in addition, the constraint (55b) may conflict with accuracy constraints as given in (49).

4.3. Discrete Wave Speed

Under the conditions (55) above, one may solve for the numerical frequency of oscillation and phase velocity as a function of wavenumber, as

$$\omega = \frac{2}{k} \sin^{-1}\left(\frac{\lambda}{2}\sqrt{-\frac{\hat{D}_{\mathcal{Q}^{(e)}, \boldsymbol{\alpha}^{(e)}}\left(\boldsymbol{\zeta}\right)}{1 + D_{\mathcal{Q}^{(i)}, \boldsymbol{\alpha}^{(i)}}\left(\boldsymbol{\zeta}\right)}}\right) \qquad\qquad v_\phi = \frac{\omega}{|\boldsymbol{\zeta}|} \,. \tag{57}$$

Under conditions for $2M$th-order accuracy, the modified equation representation (53) leads directly to the characteristic equation

$$P\left(\omega, \boldsymbol{\zeta}\right) = O(k^{2M}) \,, \tag{58}$$

The error expression consists of product terms of even powers of ω and the components of $\boldsymbol{\zeta}$, of minimal order $2M+2$. Using (58), this may be written as

$$-\omega^2 + |\boldsymbol{\zeta}|^2 = \sum_{m=M+1}^{\infty} \frac{k^{2m-2}}{\lambda^{2m-2}} \Upsilon_m |\boldsymbol{\zeta}|^{2m} \tag{59}$$

for some residual coefficients Υ_m which depend on the angle of the wave vector, and λ, but which are independent of the time step k.

Defining normalised variables $\hat{\omega} = k\omega$ and $\hat{\boldsymbol{\zeta}} = h\boldsymbol{\zeta}$, and noting that $v_\phi = \hat{\omega}/\lambda\hat{\boldsymbol{\zeta}}$, then the characteristic equation may be rewritten as

$$v_\phi^2 = 1 - \sum_{m=M+1}^{\infty} \Upsilon_m |\hat{\boldsymbol{\zeta}}|^{2m-2} \,. \tag{60}$$

In the low frequency limit, or as $|\hat{\boldsymbol{\zeta}}|$ approaches zero,

$$v_\phi \approxeq 1 - \frac{1}{2}\Upsilon_{M+1} |\hat{\boldsymbol{\zeta}}|^{2M} \,, \tag{61}$$

which implies that in this limit, the truncation error of the scheme follows:

$$\text{Error} = 1 - v_\phi \propto |\hat{\boldsymbol{\zeta}}|^{2M} \,. \tag{62}$$

It is worth mentioning that the truncation error of the scheme follows this behaviour along all directions, whereas some previous work had only achieved this along specific directions [43].

4.4. Summary of Constraints

Consider the family of schemes (40) parametrised by $\mathcal{Q}^{(e)} = \{\mathbf{q}_1^{(e)}, \ldots, \mathbf{q}_{N^{(e)}}^{(e)}\}$ and $\mathcal{Q}^{(i)} = \{\mathbf{q}_1^{(i)}, \ldots, \mathbf{q}_{N^{(i)}}^{(i)}\}$, the index sets corresponding to the two discrete Laplacians $\delta_{\mathcal{Q}^{(e)}}$ and $\delta_{\mathcal{Q}^{(i)}}$ respectively. Thus $\text{card}\left(\mathcal{Q}^{(e)}\right) = N^{(e)}$, and $\text{card}\left(\mathcal{Q}^{(i)}\right) = N^{(i)}$, so that the total number of scheme parameters is $N = N^{(e)} + N^{(i)}$, with λ as a remaining parameter. For accuracy of the scheme to $2M$th order, it is useful to present the constraints for consistency, isotropy and accuracy in a compact form.

For consistency, the following constraint, as given in (15) must be satisfied for the parameter set $\boldsymbol{\alpha}^{(e)}$:

$$\mathbf{C}_{\text{c}}^{(e)} \boldsymbol{\alpha}^{(e)} = 1 \qquad \mathbf{C}_{\text{c}}^{(e)} = \underbrace{[1, \ldots, 1]}_{N^{(e)}} \,. \tag{63}$$

For isotropy of the Laplacian approximation $\delta_{\mathcal{Q}^{(e)}}$ to $M^{(e)}$th order, with $M^{(e)} \geq M$, the following constraints, as given in (29), must be satisfied for the parameter set $\boldsymbol{\alpha}^{(e)}$:

$$\mathbf{C}_{\text{iso}}^{(e),m} \boldsymbol{\alpha}^{(e)} = \mathbf{0} \qquad m = 2, \ldots, M^{(e)} \,. \tag{64}$$

Here, $\mathbf{C}_{\text{iso}}^{(e),m}$ is an $M^{(m)} \times N^{(e)}$ matrix, where $M^{(m)}$ is as defined in (31). The (s,p)th element of $\mathbf{C}_{\text{iso}}^{(e),m}$ is defined as

$$[\mathbf{C}_{\text{iso}}^{(e),m}]_{s,p} = \epsilon_{\mathbf{q}_p^{(e)}}^{(m)} \left(g_{\mathbf{q}_p^{(e)}}^{(\boldsymbol{\eta}_s)} - f^{(\boldsymbol{\eta}_s)} \right) \qquad s = 1, \ldots, M^{(m)}, \quad p = 1, \ldots, N^{(e)} \,, \tag{65}$$

where $\boldsymbol{\eta}_s$ is the sth vector in the set $\tilde{\mathbb{M}}^{(m)}$ as defined in (27), according to any ordering. The forms ϵ and g are as defined in (23), and f in (26).

Similarly, for isotropy of the Laplacian approximation $\delta_{\mathcal{Q}^{(i)}}$ to $M^{(i)}$th order, with $M^{(i)} \geq M-1$, the following constraints, again as given in (29), must be satisfied for the parameter set $\boldsymbol{\alpha}^{(i)}$:

$$\mathbf{C}_{\text{iso}}^{(i),m} \boldsymbol{\alpha}^{(i)} = \mathbf{0} \qquad m = 2, \ldots, M^{(i)} \,. \tag{66}$$

Here, $\mathbf{C}_{\text{iso}}^{(i),m}$ is an $M^{(m)} \times N^{(i)}$ matrix, defined similarly to $\mathbf{C}_{\text{iso}}^{(e),m}$.

For accuracy to Mth order, the following constraints, as given in (49), must be satisfied:

$$\mathbf{C}_{\text{acc}}^{(e),m}\boldsymbol{\alpha}^{(e)} - \mathbf{C}_{\text{acc}}^{(i),m}(\lambda)\,\boldsymbol{\alpha}^{(e)} = \lambda^{2m-2} \qquad m = 2,\ldots,M\,, \tag{67}$$

where the $1 \times N^{(e)}$ vector $\mathbf{C}_{\text{acc}}^{(e),m}$ and $1 \times N^{(i)}$ vector $\mathbf{C}_{\text{acc}}^{(i),m}$ are defined by

$$\mathbf{C}_{\text{acc}}^{(e),m} = [\epsilon_{\mathbf{q}_1^{(e)}}^{(m)},\ldots,\epsilon_{\mathbf{q}_{N^{(e)}}^{(e)}}^{(m)}] \qquad \mathbf{C}_{\text{acc}}^{(i),m}(\lambda) = \sum_{\xi=1}^{m-1} w_\xi^{(m)}\lambda^{2m-2\xi-2}[\epsilon_{\mathbf{q}_1^{(i)}}^{(\xi)},\ldots,\epsilon_{\mathbf{q}_{N^{(i)}}^{(i)}}^{(\xi)}]\,, \tag{68}$$

where w is as defined in (48).

The complete set of constraints may be written, in vector-matrix form, as

$$\begin{array}{l}\text{Consistency}\\ \\ \text{Isotropy of } \delta_{\mathcal{Q}^{(e)}}\\ \\ \\ \text{Isotropy of } \delta_{\mathcal{Q}^{(i)}}\\ \\ \\ \text{Accuracy}\\ \\ \\ \\ \\ \end{array}\!\!\left[\begin{array}{c|c} \mathbf{C}_{\text{c}}^{(e)} & \mathbf{0} \\ \hline \mathbf{C}_{\text{iso}}^{(e),2} & \mathbf{0} \\ \vdots & \vdots \\ \mathbf{C}_{\text{iso}}^{(e),M^{(e)}} & \mathbf{0} \\ \hline \mathbf{0} & \mathbf{C}_{\text{iso}}^{(i),2} \\ \vdots & \vdots \\ \mathbf{0} & \mathbf{C}_{\text{iso}}^{(i),M^{(i)}} \\ \hline \mathbf{C}_{\text{acc}}^{(e),2} & -\mathbf{C}_{\text{acc}}^{(i),2}(\lambda) \\ \vdots & \vdots \\ \mathbf{C}_{\text{acc}}^{(e),M} & -\mathbf{C}_{\text{acc}}^{(i),M}(\lambda) \end{array}\right]\left[\begin{array}{c} \boldsymbol{\alpha}^{(e)} \\ \hline \boldsymbol{\alpha}^{(i)} \end{array}\right] = \left[\begin{array}{c} 1 \\ \hline \mathbf{0} \\ \vdots \\ \mathbf{0} \\ \hline \mathbf{0} \\ \vdots \\ \mathbf{0} \\ \hline \lambda^2 \\ \vdots \\ \lambda^{2M-2} \end{array}\right]. \tag{69}$$

5. Examples

In this section, various examples of schemes for the wave equation in 1D, 2D and 3D are presented. Stability conditions provided alongside schemes follow from (55), which are available in closed form for schemes with a small number of parameters, but which ultimately require numerical evaluation. The purpose of this section is: (a) to illustrate how one can derive a variety of schemes with this general framework (including schemes previously derived in the literature); (b) to verify that the reported orders of accuracies are reflected in rates of convergence, using analytic solutions and in terms of the discrete wave speed; (c) to illustrate advantages of novel schemes over previously derived schemes; and (d) to highlight some of the issues and peculiarities that may arise in this framework and the associated calculations.

5.1. 1D

The wave equation in 1D allows for an exact solution with the simplest of finite difference methods [44, 45] (for a bandlimited solution [31]), and is thus not representative of the techniques described in this paper. Nonetheless, for completeness, it is useful to present various families of schemes.

A general approximation to the 1D Laplacian may be written over the set $\mathcal{G}_1^{(N)}$, consisting of the first N non-negative integers.

$$\mathcal{G}_1^{(1)} = \{[1]\}, \quad \mathcal{G}_1^{(2)} = \{[1],[2]\}, \quad \mathcal{G}_1^{(3)} = \{[1],[2],[3]\},\ldots \tag{70}$$

See Figure 2, illustrating the stencils of these families of approximations.

Figure 2: Stencils of approximations to the 1D Laplacian over $\mathcal{G}_1^{(1)}$, $\mathcal{G}_1^{(2)}$, $\mathcal{G}_1^{(3)}$ and $\mathcal{G}_1^{(4)}$.

5.1.1. Explicit Schemes

Consider first explicit schemes with $\mathcal{Q}^{(e)} = \mathcal{G}_1^{(N^{(e)})}$ and $\mathcal{Q}^{(i)} = \emptyset$, parametrised by $\alpha_1^{(e)}, \ldots, \alpha_{N^{(e)}}^{(e)}$. Isotropy constraints are trivially satisfied in this case, and, for accuracy to $2M$th order, where $M = N^{(e)}$, the constraints (15) and (49) lead to the matrix equation

$$\begin{bmatrix} 1 & 1 & 1 & \ldots & 1 \\ 1 & 2^2 & 3^2 & \ldots & (N^{(e)})^2 \\ \vdots & \vdots & \vdots & \vdots & \vdots \\ 1 & 2^{(2N^{(e)}-2)} & 3^{(2N^{(e)}-2)} & \ldots & (N^{(e)})^{(2N^{(e)}-2)} \end{bmatrix} \begin{bmatrix} \alpha_1^{(e)} \\ \vdots \\ \vdots \\ \alpha_{N^{(e)}}^{(e)} \end{bmatrix} = \begin{bmatrix} 1 \\ \lambda^2 \\ \vdots \\ \lambda^{2N^{(e)}-2} \end{bmatrix} . \tag{71}$$

This Vandermonde system has the solution

$$\alpha_p^{(e)} = \prod_{q=1, q\neq p}^{N^{(e)}} \frac{\lambda^2 - q^2}{p^2 - q^2} , \tag{72}$$

resulting in a scheme that has appeared in the literature previously in various equivalent forms [46, 47, 31, 8]. Furthermore, it has been shown that this scheme is stable for $\lambda \leq 1$ [46, 47]. Notice in particular that the scheme coefficients are polynomials in λ^2, a feature which will persist in all higher-order designs in higher dimensions.

Under the special choice of $\lambda = 1$, the solution reduces to

$$\alpha_1^{(e)} = 1 \qquad \text{and} \qquad \alpha_p^{(e)} = 0, \quad \text{for} \quad p > 1 . \tag{73}$$

That is, the scheme reduces to the simplest possible explicit scheme for the 1D wave equation—that defined over $\mathcal{G}_1^{(1)}$ (dating back to [7]). Furthermore, this reduction to the exact scheme holds regardless of the order $2M$ of accuracy, and thus the scheme can be viewed as of infinite order, or exact (and indeed is a known special case [44, 45]).

This scheme is pathological in the present context, as an exact numerical solution is available, relying on a special choice of the Courant number λ. In the remainder of this work, the parameter λ, though constrained in a complex way by conditions for both accuracy and stability, will be allowed to remain as an at least partially free parameter—that is, it may take on values over a continuum, but is normally bounded (usually from above, but in some cases from below as well).

See Figure 3, showing phase velocity as a function of normalised wavenumber, for schemes of different orders of accuracy O. Increased flatness with M is visible in error plots—on a doubly logarithmic scale, the accuracy of the scheme is manifested as a slope $2M$ of the error curve in the limit of small wavenumber, as per (62).

5.1.2. Implicit Schemes

Though, as mentioned above, an exact explicit scheme is available, it is useful to also present some implicit schemes for the 1D wave equation, in order to indicate some of the issues which will emerge in higher dimensions. Consider now implicit schemes with $\mathcal{Q}^{(e)} = \mathcal{G}_1^{(N^{(e)})}$ and $\mathcal{Q}^{(i)} = \mathcal{G}_1^{(N^{(i)})}$. For $2M$th order accuracy, it is required that $N^{(e)} + N^{(i)} \geq M$. In contrast to the case of explicit schemes, a complete characterisation of all such implicit schemes is more difficult in this case, and thus representative examples will be presented below.

Choosing $N^{(e)} = 1$ and $N^{(i)} = 1$, and employing a consistency constraint as well as a condition for fourth-order accuracy leads to the system

$$\begin{bmatrix} 1 & 0 \\ 1 & -12 \end{bmatrix} \begin{bmatrix} \alpha_1^{(e)} \\ \alpha_1^{(i)} \end{bmatrix} = \begin{bmatrix} 1 \\ \lambda^2 \end{bmatrix} \qquad \Rightarrow \qquad \alpha_1^{(e)} = 1, \quad \alpha_1^{(i)} = \frac{1 - \lambda^2}{12} \tag{74}$$

which is a well-known special case of von Neumann's implicit scheme [48]. The stability condition for this scheme may be calculated easily as $\lambda \leq 1$. When $\lambda = 1$, an explicit scheme results, which has been shown above to be exact.

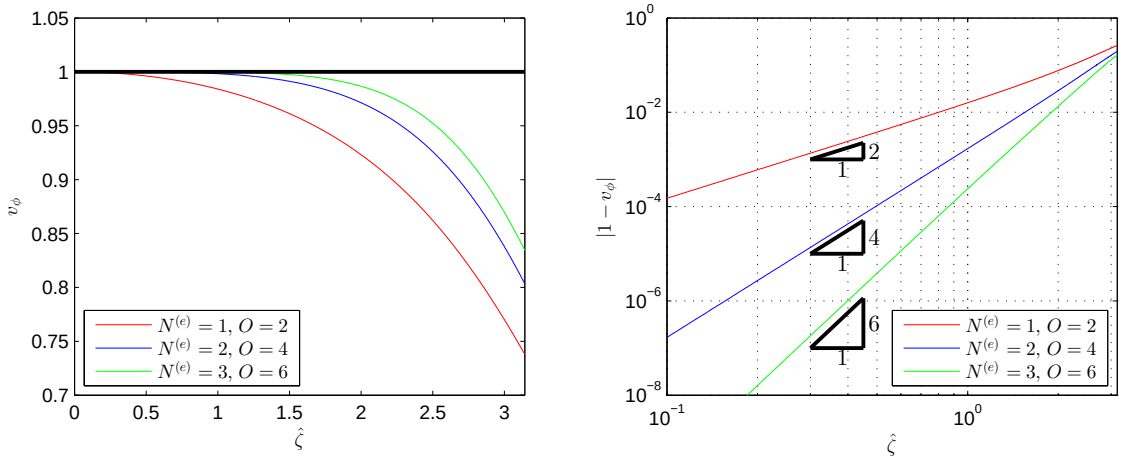

Figure 3: Phase velocity v_ϕ (left) and error (right) as a function of normalised wavenumber $\hat{\zeta}$, for explicit higher order accurate schemes for the 1D wave equation with $\lambda = 0.8$, as described in Section 5.1.1. The order of accuracy is indicated by O.

Choosing $N^{(e)} = 2$ and $N^{(i)} = 1$, and employing a consistency constraint as well as conditions for sixth-order accuracy leads to the system

$$\begin{bmatrix} 1 & 1 & 0 \\ 1 & 4 & -12 \\ 1 & 16 & -30\left(1+\lambda^2\right) \end{bmatrix} \begin{bmatrix} \alpha_1^{(e)} \\ \alpha_2^{(e)} \\ \alpha_1^{(i)} \end{bmatrix} = \begin{bmatrix} 1 \\ \lambda^2 \\ \lambda^4 \end{bmatrix} \quad \Rightarrow \quad \alpha_1^{(e)} = \frac{4-\lambda^2}{5}, \quad \alpha_2^{(e)} = \frac{1+\lambda^2}{5}, \quad \alpha_1^{(i)} = \frac{4-\lambda^2}{30} \tag{75}$$

The stability condition for this novel scheme may be calculated as $\lambda \leq 1$. As before, for $\lambda = 1$, a simple exact explicit scheme results. An additional stable scheme is available for $\lambda = 2$, in which case the scheme reduces to an explicit scheme over a spatial grid of spacing $2h$.

A different sixth-order accurate implicit scheme results when $N^{(e)} = 1$ and $N^{(i)} = 2$. The constraints may be written as

$$\begin{bmatrix} 1 & 0 & 0 \\ 1 & -12 & -12 \\ 1 & -30\left(1+\lambda^2\right) & -30\left(4+\lambda^2\right) \end{bmatrix} \begin{bmatrix} \alpha_1^{(e)} \\ \alpha_1^{(i)} \\ \alpha_2^{(i)} \end{bmatrix} = \begin{bmatrix} 1 \\ \lambda^2 \\ \lambda^4 \end{bmatrix} \quad \Rightarrow \quad \alpha_1^{(e)} = 1\,, \quad \boldsymbol{\alpha}^{(i)} = \frac{1}{60}\left[6-5\lambda^2-\lambda^4\,, \quad -1+\lambda^4\right]^{\mathrm{T}} \tag{76}$$

This novel scheme is also stable for $\lambda \leq 1$, and reduces to the exact explicit scheme when $\lambda = 1$. See Figure 4.

5.1.3. Numerical Results

As a basic numerical test illustrating rates of convergence for the schemes presented here, consider the problem of the 1D wave equation, over the periodic domain $x \in [-1/2, 1/2)$, and with initial data $v_0(x) = \exp\left(-x^2/2\sigma^2\right)$, and with $v_1(x) = 0$. The various schemes presented here may be initialised, at the first two time steps, with exact values of the solution, sampled over the grid. For a given duration T, simulated values are generated under refinement of the time step k, assumed to subdivide T evenly; the grid spacing h is set as $h = k/\lambda$, for fixed Courant number λ. If the calculated values are written as $u_l^{(\mathrm{sim})}$, and exact values, obtained from samples of the solution at time T are written as $u_l^{(\mathrm{ex})}$, for $l \in \mathbb{D}(k)$, where $\mathbb{D}(k)$ is the finite set of grid indices over which the solution is computed for a given time step k, then the relative L_2 error may be written as

$$E(k) = \sqrt{\frac{\sum_{l\in\mathbb{D}(k)}\left(u_l^{(\mathrm{ex})} - u_l^{(\mathrm{sim})}\right)^2}{\sum_{l\in\mathbb{D}(k)}\left(u_l^{(\mathrm{ex})}\right)^2}}\,. \tag{77}$$

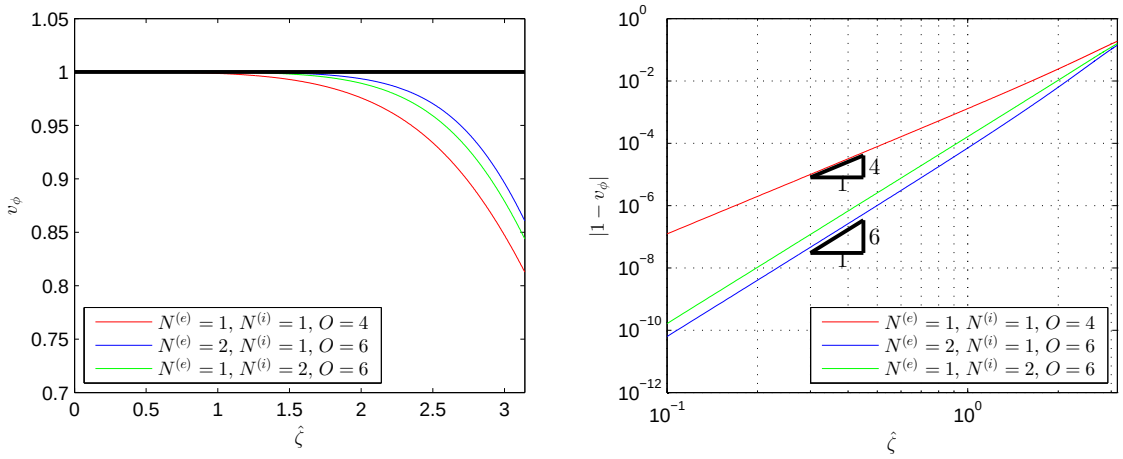

Figure 4: Phase velocity v_ϕ (left) and error (right) as a function of normalised wavenumber $\hat{\zeta}$, for implicit higher order accurate schemes for the 1D wave equation with $\lambda = 0.8$, as described in Section 5.1.2.

See Figure 5. Note that while errors are plotted as a function of the time step k, the grid spacing h is refined at the same rate as the time step k in these experiments—i.e., the Courant number is kept constant for each respective scheme.

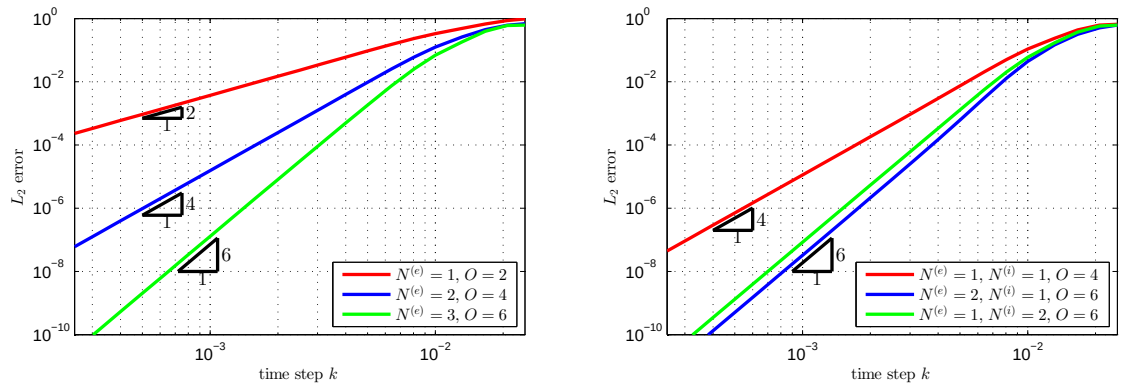

Figure 5: Relative L_2 error $E(k)$, as defined in (77), as a function of k, the time step, on a doubly logarithmic scale, for the test problem as described at the beginning of Section 5.1.3, with $\sigma = 0.0129$ and $T = 0.25$. The Courant number is chosen as $\lambda = 0.8$ in all cases. Left: for the explicit schemes, with coefficients as given in (72), as described in Section 5.1.1, to various orders of accuracy. Right: for the implicit schemes as described in Section 5.1.2.

5.2. 2D

A general approximation to the 2D Laplacian may be written over the set $\mathcal{G}_2^{(N)}$, consisting of the first N admissible 2-vectors.

$$\mathcal{G}_2^{(1)} = \{[1,0]\}, \quad \mathcal{G}_2^{(2)} = \{[1,0],[1,1]\}, \quad \mathcal{G}_2^{(3)} = \{[1,0],[1,1],[2,0]\}, \ldots \tag{78}$$

See Figure 6, illustrating the stencils of these families of approximations.

5.2.1. General Explicit Schemes

Consider first explicit schemes with $\mathcal{Q}^{(e)} = \mathcal{G}_2^{(N^{(e)})}$ and $\mathcal{Q}^{(i)} = \emptyset$.

When $N^{(e)} = 1$, the simplest possible scheme for the 2D wave equation results [7], sometimes referred to as the five-point explicit scheme; here, $\alpha_1^{(e)} = 1$, and no isotropy or accuracy constraints may be employed. The well-known stability condition for this scheme is $\lambda \leq 1/\sqrt{2} \approx 0.707$. This is also the first in a family

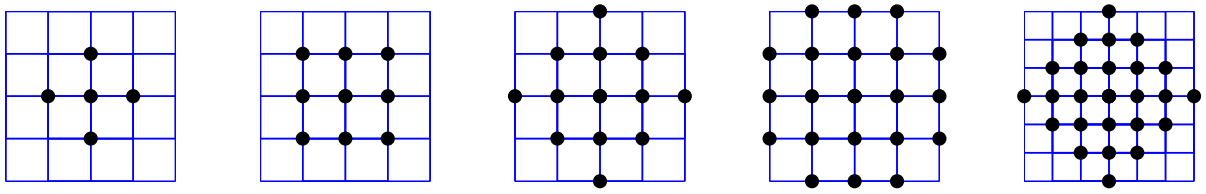

Figure 6: Stencils of approximations to the 2D Laplacian over $\mathcal{G}_2^{(1)}$, $\mathcal{G}_2^{(2)}$, $\mathcal{G}_2^{(3)}$, $\mathcal{G}_2^{(4)}$ and $\mathcal{G}_2^{(5)}$.

of schemes using stencils that are spatially compact in a L^1-sense—henceforth "diamond-shaped" shaped stencils—which includes the examples $\mathcal{G}_2^{(2)}$ and $\mathcal{G}_2^{(5)}$ in Fig. 6. See also Figure 7, illustrating the numerical phase velocity characteristics of this scheme.

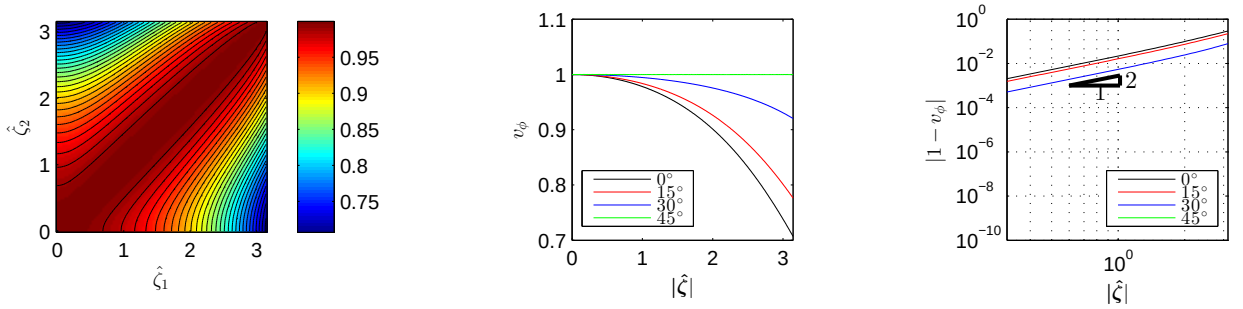

Figure 7: Numerical phase velocity of the simplest explicit scheme for the 2D wave equation, with $N^{(e)} = 1$, and at the stability limit $\lambda = 1/\sqrt{2}$. Left: 1% contours. Middle: as a function of wavenumber, for various angles, as indicated. Right: error as a function of wavenumber, for various angles, as indicated.

When $N^{(e)} = 2$, a nine-point scheme results [49]. Again, no high-order accuracy constraints may be employed here, but a consistency constraint as well as a condition for fourth-order isotropy leads to the system

$$\begin{bmatrix} 1 & 1 \\ -1 & 2 \end{bmatrix} \begin{bmatrix} \alpha_1^{(e)} \\ \alpha_2^{(e)} \end{bmatrix} = \begin{bmatrix} 1 \\ 0 \end{bmatrix} \qquad \Rightarrow \qquad \boldsymbol{\alpha}^{(e)} = \begin{bmatrix} \frac{2}{3}, & \frac{1}{3} \end{bmatrix}^{\mathrm{T}} \tag{79}$$

The stability condition for this scheme may be calculated easily as $\lambda \leq \sqrt{3}/2 \approx 0.866$. See Figure 8.

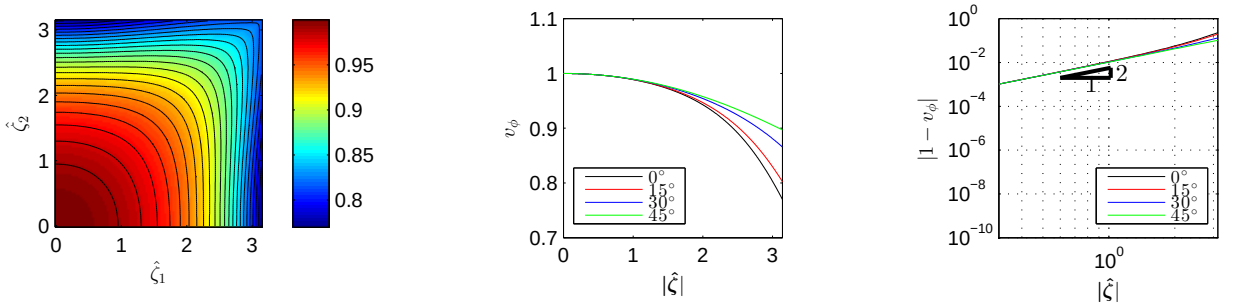

Figure 8: Numerical phase velocity of the explicit scheme for the 2D wave equation, with $N^{(e)} = 2$, and with isotropy to fourth order at the stability limit $\lambda = \sqrt{3}/2$. Left: 1% contours. Middle: as a function of wavenumber, for various angles, as indicated. Right: error as a function of wavenumber, for various angles, as indicated.

When $N^{(e)} = 3$, a thirteen-point scheme results, employing the stencil $\mathcal{G}_2^{(3)}$ illustrated in Fig. 6. Em-

ploying conditions for consistency, fourth-order isotropy, and fourth-order accuracy leads to the system

$$\begin{bmatrix} 1 & 1 & 1 \\ 1 & -2 & 4 \\ 1 & 1 & 4 \end{bmatrix} \begin{bmatrix} \alpha_1^{(e)} \\ \alpha_2^{(e)} \\ \alpha_3^{(e)} \end{bmatrix} = \begin{bmatrix} 1 \\ 0 \\ \lambda^2 \end{bmatrix} \qquad \Rightarrow \qquad \boldsymbol{\alpha}^{(e)} = \frac{1}{3}\begin{bmatrix} 4-2\lambda^2\,, & \lambda^2\,, & \lambda^2-1 \end{bmatrix}^{\mathrm{T}} \tag{80}$$

This scheme, which is well-known [27, 30, 8], is stable under the condition $\lambda \leq 1/\sqrt{2}$ [30]. This scheme represents the second of the diamond-shaped family of schemes; the first being the simplest scheme. See also Figure 9.

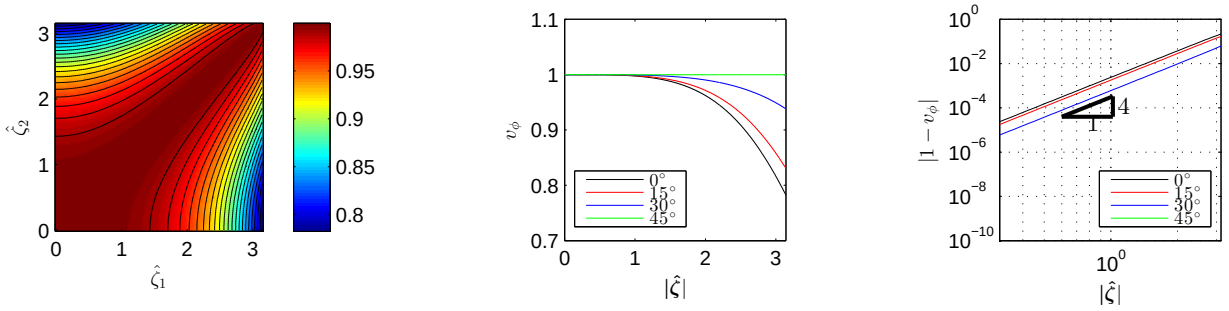

Figure 9: Numerical phase velocity of the fourth-order accurate explicit scheme for the 2D wave equation, with $N^{(e)} = 3$, at the stability limit $\lambda = 1/\sqrt{2}$. Left: 1% contours. Middle: as a function of wavenumber, for various angles, as indicated. Right: error as a function of wavenumber, for various angles, as indicated.

When $N^{(e)} = 4$, a 21-point scheme results, employing the stencil $\mathcal{G}_2^{(4)}$ illustrated in Fig. 6. In this case, there are not enough free parameters to permit a sixth-order accurate scheme. It is useful, however, to examine the extended family of fourth-order accurate schemes which results. Employing the conditions for consistency, fourth-order isotropy, and fourth-order accuracy leads to the underdetermined system

$$\begin{bmatrix} 1 & 1 & 1 & 1 \\ 1 & -2 & 4 & -7/5 \\ 1 & 1 & 4 & 17/5 \end{bmatrix} \begin{bmatrix} \alpha_1^{(e)} \\ \alpha_2^{(e)} \\ \alpha_3^{(e)} \\ \alpha_4^{(e)} \end{bmatrix} = \begin{bmatrix} 1 \\ 0 \\ \lambda^2 \end{bmatrix} \tag{81}$$

Taking $b = \alpha_3^{(e)}$ as a free parameter, the scheme parameters may be written as

$$\boldsymbol{\alpha}^{(e)} = \left[-\frac{7b}{4} + \frac{1}{12}\left(9-\lambda^2\right)\,, \quad 2b + \frac{1}{3}\left(2-\lambda^2\right)\,, \quad b\,, \quad -\frac{5b}{4} + \frac{5}{12}\left(\lambda^2-1\right) \right]^{\mathrm{T}} \tag{82}$$

The determination of stability conditions is more involved in this case. See Figure 10 for an illustration of the stability region of this family of schemes as a function of the free parameters b and λ^2. The scheme will be stable, for some values of $\lambda > 0$, when $b \leq 1/3$. $\lambda \leq 1$ is required for stability for any member of this family.

Various special choices of the parameter b are of interest. When $b = \left(\lambda^2 - 1\right)/3$, the fourth-order accurate scheme defined above over $\mathcal{G}_2^{(3)}$ results. If the additional constraint of sixth-order isotropy is employed, then the value of b is set to $b = \lambda^2/9 - 1/15$. The scheme will be stable under the condition $\lambda \leq \sqrt{\frac{3}{10}(6-\sqrt{11})} \approx 0.897$ in this case (a known special case [50]). Finally, when $b = 0$, a fourth-order accurate scheme operating over a reduced stencil consisting only of the three Laplacian shells $\mathcal{Q} = \{[1,0],[1,1],[2,1]\}$ results, and is stable for $\lambda \leq \sqrt{3}/2 \approx 0.866$ [51]. See Figure 11. While these fourth-order accurate schemes use more points than the 13-point diamond-shaped scheme, they have the advantage of a higher Courant number than the 13-point scheme ($\lambda \leq 1/\sqrt{2} \approx 0.707$), and thus fewer time-steps need to calculated for a fixed duration and grid resolution. It is worth recalling that the operations carried out at each point and time-step can be carried out in parallel, yet time-stepping is inherently sequential; thus, the benefits of having a higher time-step will generally outweigh the additional operations required at each time-step. Additionally, comparing

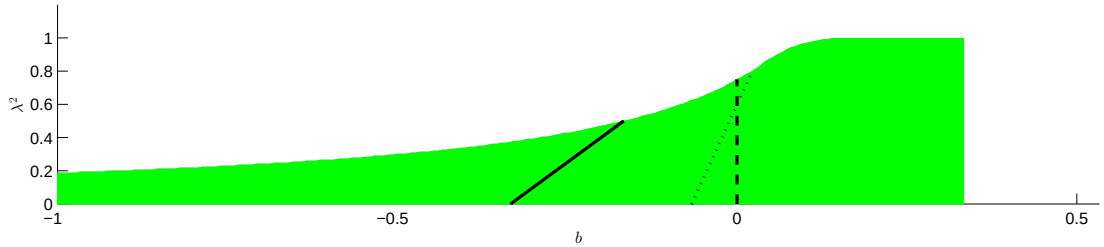

Figure 10: Stability region, in green, evaluated numerically for fourth-order accurate schemes defined over $\mathcal{G}_2^{(4)}$, as a function of free parameter $b = \alpha_3^{(e)}$ and λ^2. Special cases of the stability ranges are shown for the fourth-order accurate scheme defined over $\mathcal{G}_2^{(4)}$ (solid black line), for a sixth-order isotropic scheme (dotted black line) and for a scheme over the reduced stencil $\mathcal{Q} = \{[10], [11], [21]\}$ (dashed black line).

the contour plots in Figs. 9 and 11, it can be seen that the first 2% error contours for these schemes appear at higher wavenumbers than for the 13-point scheme, meaning that if a given application permits such an error tolerance, these schemes will benefit from employing coarser spatial grids.

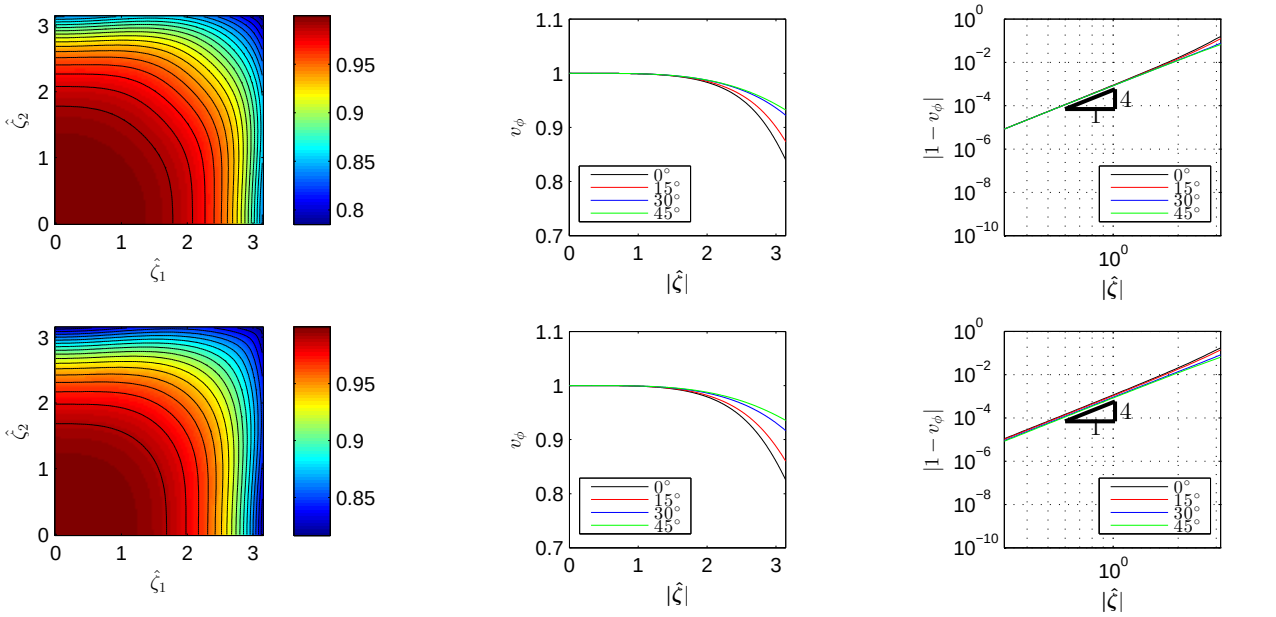

Figure 11: Numerical phase velocity of the parametrised fourth-order accurate explicit scheme for the 2D wave equation, with $N^{(e)} = 4$. Top row: when a sixth-order isotropy condition is employed. Bottom row: over a reduced stencil. The Courant number λ is chosen at the stability limit in both cases. Left: 1% contours. Middle: as a function of wavenumber, for various angles, as indicated. Right: error as a function of wavenumber, for various angles, as indicated.

When $N^{(e)} = 5$, a 25-point scheme results, employing the stencil $\mathcal{G}_2^{(5)}$ illustrated in Fig. 6. In this case, one can impose constraints of sixth-order accuracy to yield the system

$$\begin{bmatrix} 1 & 1 & 1 & 1 & 1 \\ 1 & -2 & 4 & -\frac{7}{5} & 9 \\ 1 & -4 & 16 & -7 & 81 \\ 1 & 1 & 4 & \frac{17}{5} & 9 \\ 1 & 1 & 16 & 13 & 81 \end{bmatrix} \begin{bmatrix} \alpha_1^{(e)} \\ \alpha_2^{(e)} \\ \alpha_3^{(e)} \\ \alpha_4^{(e)} \\ \alpha_5^{(e)} \end{bmatrix} = \begin{bmatrix} 1 \\ 0 \\ 0 \\ \lambda^2 \\ \lambda^4 \end{bmatrix} \quad \Rightarrow \quad \boldsymbol{\alpha}^{(e)} = \begin{bmatrix} \frac{3}{2} \\ 0 \\ -\frac{3}{5} \\ 0 \\ \frac{1}{10} \end{bmatrix} + \begin{bmatrix} -\frac{77}{72} \\ \frac{5}{9} \\ \frac{7}{9} \\ -\frac{5}{36} \\ -\frac{1}{8} \end{bmatrix} \lambda^2 + \begin{bmatrix} \frac{19}{120} \\ -\frac{2}{15} \\ -\frac{2}{15} \\ \frac{1}{12} \\ \frac{1}{40} \end{bmatrix} \lambda^4 \tag{83}$$

This scheme is the third of the diamond family of schemes and has been previously derived in [30, 8]. It is

stable for $\lambda \leq 1/\sqrt{2}$. See also Figure 12.

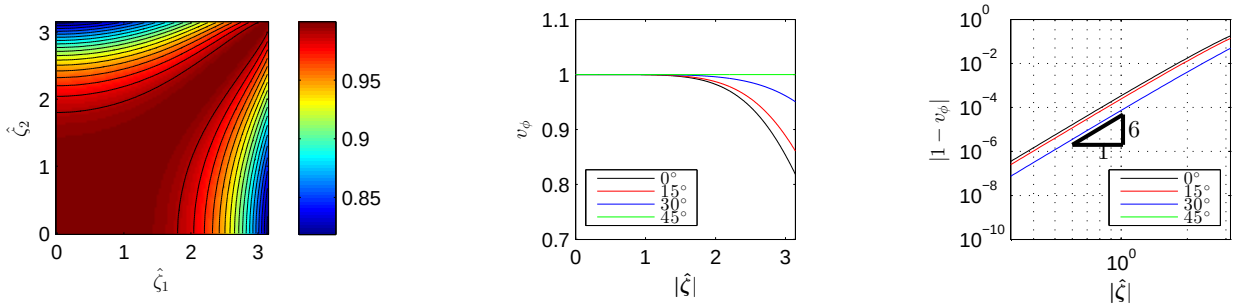

Figure 12: Numerical phase velocity of the sixth-order accurate explicit scheme for the 2D wave equation, with $N^{(e)} = 5$, at the stability lmit $\lambda = 1/\sqrt{2}$. Left: 1% contours. Middle: as a function of wavenumber, for various angles, as indicated. Right: error as a function of wavenumber, for various angles, as indicated.

For $N^{(e)} = 8$, a 41-point scheme results, and in the interest of further examining the properties of parametrised schemes, consider such a scheme constrained to sixth-order accuracy, and with conditions of eighth-order isotropy enforced, leading to

$$\begin{bmatrix} 1 & 1 & 1 & 1 & 1 & 1 & 1 & 1 \\ 1 & -2 & 4 & -\frac{7}{5} & 9 & -8 & \frac{14}{5} & 16 \\ 1 & -4 & 16 & -7 & 81 & -64 & 28 & 256 \\ 1 & -6 & 64 & -\frac{219}{5} & 729 & -384 & \frac{698}{5} & 4096 \\ 1 & -\frac{32}{3} & 64 & -\frac{349}{15} & 729 & -\frac{2048}{3} & \frac{2336}{5} & 4096 \\ 1 & 1 & 4 & \frac{17}{5} & 9 & 4 & \frac{41}{5} & 16 \\ 1 & 1 & 16 & 13 & 81 & 16 & 73 & 256 \end{bmatrix} \begin{bmatrix} \alpha_1^{(e)} \\ \alpha_2^{(e)} \\ \alpha_3^{(e)} \\ \alpha_4^{(e)} \\ \alpha_5^{(e)} \\ \alpha_6^{(e)} \\ \alpha_7^{(e)} \\ \alpha_8^{(e)} \end{bmatrix} = \begin{bmatrix} 1 \\ 0 \\ 0 \\ 0 \\ 0 \\ \lambda^2 \\ \lambda^4 \end{bmatrix} \tag{84}$$

For this underdetermined system, let the final parameter remain as free, so $b = \alpha_8^{(e)}$. The resulting solution may be written as

$$\begin{bmatrix} \alpha_1^{(e)} \\ \alpha_2^{(e)} \\ \alpha_3^{(e)} \\ \alpha_4^{(e)} \\ \alpha_5^{(e)} \\ \alpha_6^{(e)} \\ \alpha_7^{(e)} \end{bmatrix} = \begin{bmatrix} \frac{31}{35} \\ \frac{27}{35} \\ 0 \\ -\frac{6}{7} \\ -\frac{1}{35} \\ \frac{3}{35} \\ \frac{1}{7} \end{bmatrix} + \begin{bmatrix} -\frac{191}{540} \\ -\frac{187}{540} \\ \frac{7}{90} \\ \frac{47}{54} \\ \frac{1}{60} \\ -\frac{29}{270} \\ -\frac{17}{108} \end{bmatrix} \lambda^2 + \begin{bmatrix} \frac{1}{45} \\ \frac{7}{180} \\ 0 \\ -\frac{1}{9} \\ 0 \\ \frac{1}{45} \\ \frac{1}{36} \end{bmatrix} \lambda^4 + \begin{bmatrix} -25 \\ 27 \\ 28 \\ -30 \\ -9 \\ 3 \\ 5 \end{bmatrix} b \tag{85}$$

Various choices of the free parameter b lead to operation over stencils which are missing one of the Laplacian shells in the set $\mathcal{G}^{(8)}$. See Figure 13. When $b = 0$, a novel scheme over $\mathcal{G}^{(7)}$ (i.e., $\mathcal{G}^{(8)}$ without a Laplacian approximation for $\mathbf{q} = [4, 0]$) results, which is stable for $\lambda \leq 0.933$. When $b = -1/35 + 17\lambda^2/540 - \lambda^4/180$, a novel scheme over $\mathcal{G}^{(8)}$, but without a Laplacian approximation for $\mathbf{q} = [3, 1]$ results, which is stable for $\lambda \leq 0.661$. This particular scheme permits wave propagation with $v_\phi > 1$ for a certain range of wavenumbers.

Under conditions for eighth-order accuracy, a single scheme results, with the parameters b set as

$$b = -\frac{1}{35} + \frac{7}{180}\lambda^2 - \frac{1}{90}\lambda^4 + \frac{1}{1260}\lambda^6 \tag{86}$$

As this is the fourth in the diamond family of schemes, it is stable for $\lambda \leq 1/\sqrt{2}$ [30, 8]. See Figure 14.

In comparison to this eighth-order accurate diamond scheme (shown in bottom row of Figure 14), it is worth remarking that the novel sixth-order accurate, eighth-order isotropic scheme (with parameters given

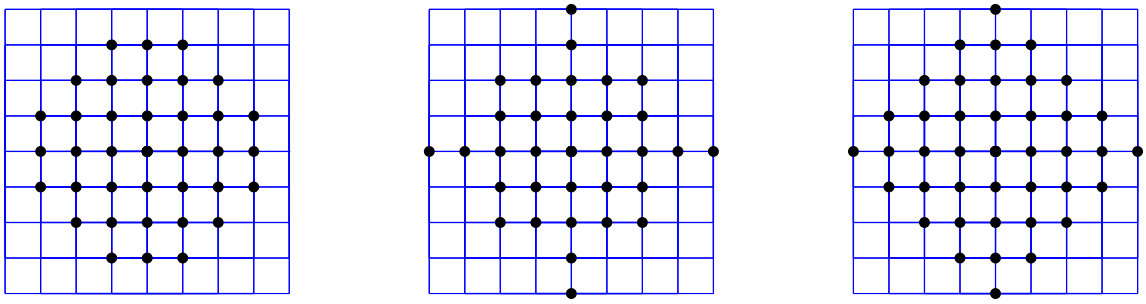

Figure 13: Stencils of approximations to the 2D Laplacian over $\mathcal{G}_2^{(7)}$ (left), $\mathcal{G}_2^{(8)}$ without Laplacian approximation [31] (center) and $\mathcal{G}_2^{(8)}$ (right).

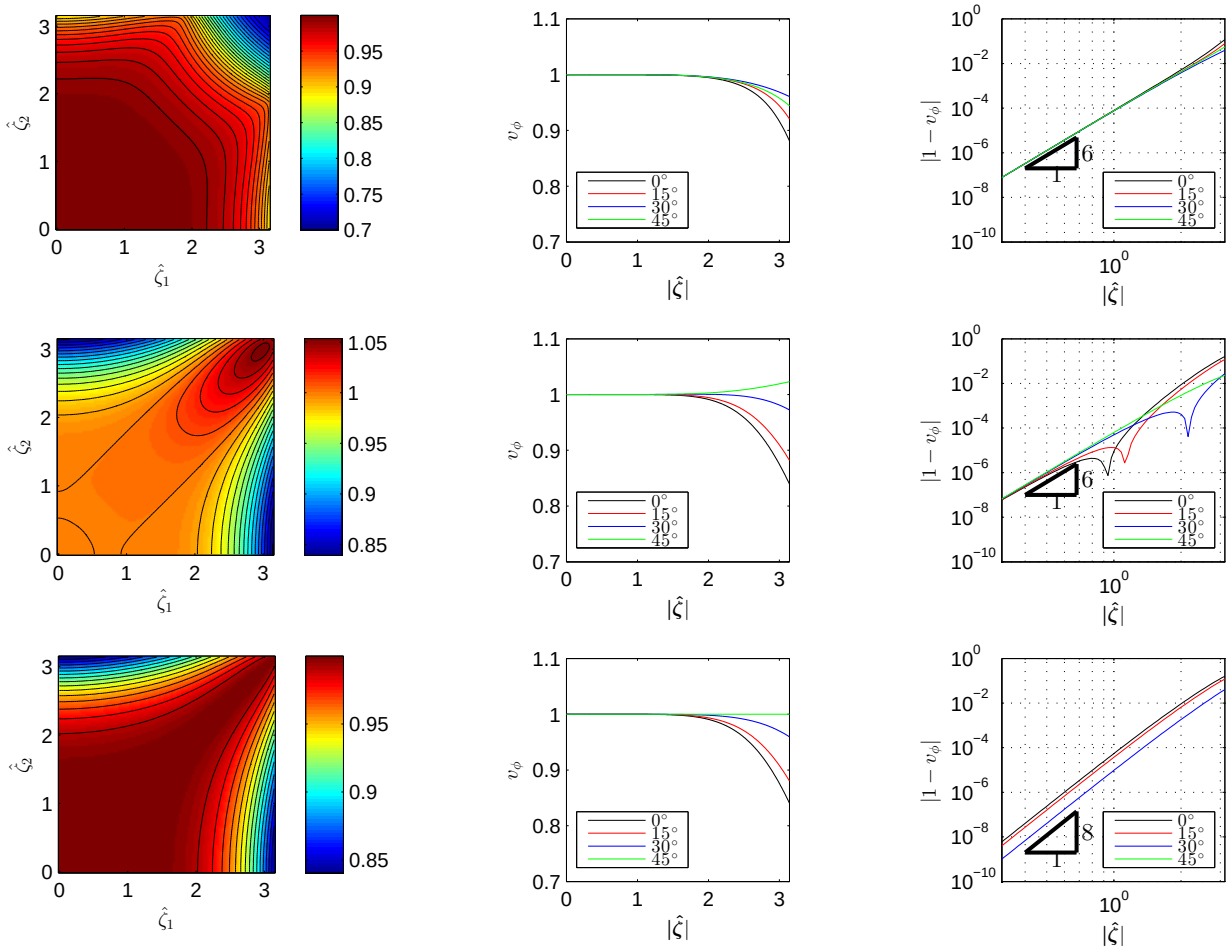

Figure 14: Numerical phase velocity of the parametrised sixth-order accurate and eighth-order isotropic explicit scheme for the 2D wave equation, with $N^{(e)} = 8$. Top row: over reduced stencil with $N^{(e)} = 7$. Middle row: over $\mathcal{G}_2^{(8)}$ without Laplacian approximation [31]. Bottom: when a condition for eighth-order accuracy is employed. The Courant number λ is chosen at the stability limit in all cases. Left: 1% contours. Middle: as a function of wavenumber, for various angles, as indicated. Right: error as a function of wavenumber magnitude, for various angles, as indicated.

by (85), and seen in the top row of Figure 14) has a significantly more favourable stability condition and a much wider region under which 2% error is achieved. Indeed, though the correct orders of accuracy are as illustrated in the third column of Figure 14, it is easy to see that beyond this measure of scheme performance,

depending on the choice of stencil, there is a great deal of variability in the ultimate performance of the scheme over the complete range of wavenumbers, as illustrated in the first and second columns of the figure.

5.2.2. Implicit Schemes

Consider now implicit 2D schemes with $\mathcal{Q}^{(e)} = \mathcal{G}_2^{(N^{(e)})}$ and $\mathcal{Q}^{(i)} = \mathcal{G}_2^{(N^{(i)})}$; in general, $N^{(e)} \neq N^{(i)}$. Such schemes have the advantage of increased order of accuracy for relatively small stencils.

The simplest scheme of fourth-order accuracy results from the choice of $N^{(e)} = 2$ and $N^{(i)} = 1$. Here, the constraints may be written as

$$\begin{bmatrix} 1 & 1 & 0 \\ 1 & -2 & 0 \\ 1 & 1 & -12 \end{bmatrix} \begin{bmatrix} \alpha_1^{(e)} \\ \alpha_2^{(e)} \\ \alpha_1^{(i)} \end{bmatrix} = \begin{bmatrix} 1 \\ 0 \\ \lambda^2 \end{bmatrix} \qquad \Rightarrow \qquad \boldsymbol{\alpha}^{(e)} = \begin{bmatrix} \frac{2}{3}, & \frac{1}{3} \end{bmatrix}^{\mathrm{T}}, \quad \alpha_1^{(i)} = \frac{1-\lambda^2}{12} \tag{87}$$

This implicit scheme is a special case of an implicit family of schemes that appears in [52]. It is stable for $\lambda \leq 1/\sqrt{2}$. See Figure 15.

For sixth-order accuracy, there are six constraints, leading to various stencil configurations. Considering first the case of $N^{(e)} = N^{(i)} = 3$, the following system results:

$$\begin{bmatrix} 1 & 1 & 1 & 0 & 0 & 0 \\ 1 & -2 & 4 & 0 & 0 & 0 \\ 1 & -4 & 12 & 0 & 0 & 0 \\ 0 & 0 & 0 & 1 & -2 & 4 \\ 1 & 1 & 4 & -12 & -12 & -12 \\ 1 & 1 & 16 & 30\left(1+\lambda^2\right) & 30\left(1+\lambda^2\right) & 30\left(4+\lambda^2\right) \end{bmatrix} \begin{bmatrix} \alpha_1^{(e)} \\ \alpha_2^{(e)} \\ \alpha_3^{(e)} \\ \alpha_1^{(i)} \\ \alpha_2^{(i)} \\ \alpha_3^{(i)} \end{bmatrix} = \begin{bmatrix} 1 \\ 0 \\ 0 \\ 0 \\ \lambda^2 \\ \lambda^4 \end{bmatrix} \tag{88}$$

leading to the choices

$$\boldsymbol{\alpha}^{(e)} = \begin{bmatrix} \frac{8}{15}, & \frac{2}{5}, & \frac{1}{15} \end{bmatrix}^{\mathrm{T}}, \quad \boldsymbol{\alpha}^{(i)} = \begin{bmatrix} \frac{4}{45} - \frac{2}{45}\lambda^2 - \frac{1}{30}\lambda^4, & \frac{1}{45} - \frac{1}{30}\lambda^2 + \frac{1}{60}\lambda^4, & -\frac{1}{90} - \frac{1}{180}\lambda^2 + \frac{1}{60}\lambda^4 \end{bmatrix}^{\mathrm{T}} \tag{89}$$

This novel scheme is stable for $\lambda \leq 1/\sqrt{2}$. See Figure 15.

Another possibility, for sixth-order accuracy, is to use $N^{(e)} = 4$ and $N^{(i)} = 2$, leading to the constraints

$$\begin{bmatrix} 1 & 1 & 1 & 1 & 0 & 0 \\ 1 & -2 & 4 & -\frac{7}{5} & 0 & 0 \\ 1 & -4 & 16 & -7 & 0 & 0 \\ 0 & 0 & 0 & 0 & 1 & -2 \\ 1 & 1 & 4 & \frac{17}{5} & -12 & -12 \\ 1 & 1 & 16 & 13 & -30\left(1+\lambda^2\right) & -30\left(1+\lambda^2\right) \end{bmatrix} \begin{bmatrix} \alpha_1^{(e)} \\ \alpha_2^{(e)} \\ \alpha_3^{(e)} \\ \alpha_4^{(e)} \\ \alpha_1^{(i)} \\ \alpha_2^{(i)} \end{bmatrix} = \begin{bmatrix} 1 \\ 0 \\ 0 \\ 0 \\ \lambda^2 \\ \lambda^4 \end{bmatrix} \tag{90}$$

leading to a novel scheme with the choices

$$\boldsymbol{\alpha}^{(e)} = \begin{bmatrix} \frac{19}{45} - \frac{1}{6}\lambda^2, & \frac{16}{45} - \frac{1}{15}\lambda^2, & \frac{1}{9} + \frac{1}{15}\lambda^2, & \frac{1}{9} + \frac{1}{6}\lambda^2 \end{bmatrix}^{\mathrm{T}}, \quad \boldsymbol{\alpha}^{(i)} = \begin{bmatrix} \frac{4}{45} - \frac{1}{45}\lambda^2, & \frac{2}{45} - \frac{1}{90}\lambda^2 \end{bmatrix}^{\mathrm{T}} \tag{91}$$

See Figure 15.

5.2.3. Schemes over Star-shaped Stencils

A specialised approximation to the 2D Laplacian may be written over the set $\mathcal{S}_2^{(N)}$, consisting of the first N admissible 2-vectors for which the second component is 0:

$$\mathcal{S}_2^{(1)} = \{[1\ 0]\}, \quad \mathcal{S}_2^{(2)} = \{[1\ 0], [2\ 0]\}, \quad \mathcal{S}_2^{(3)} = \{[1\ 0], [2\ 0], [3\ 0]\}, \ldots \tag{92}$$

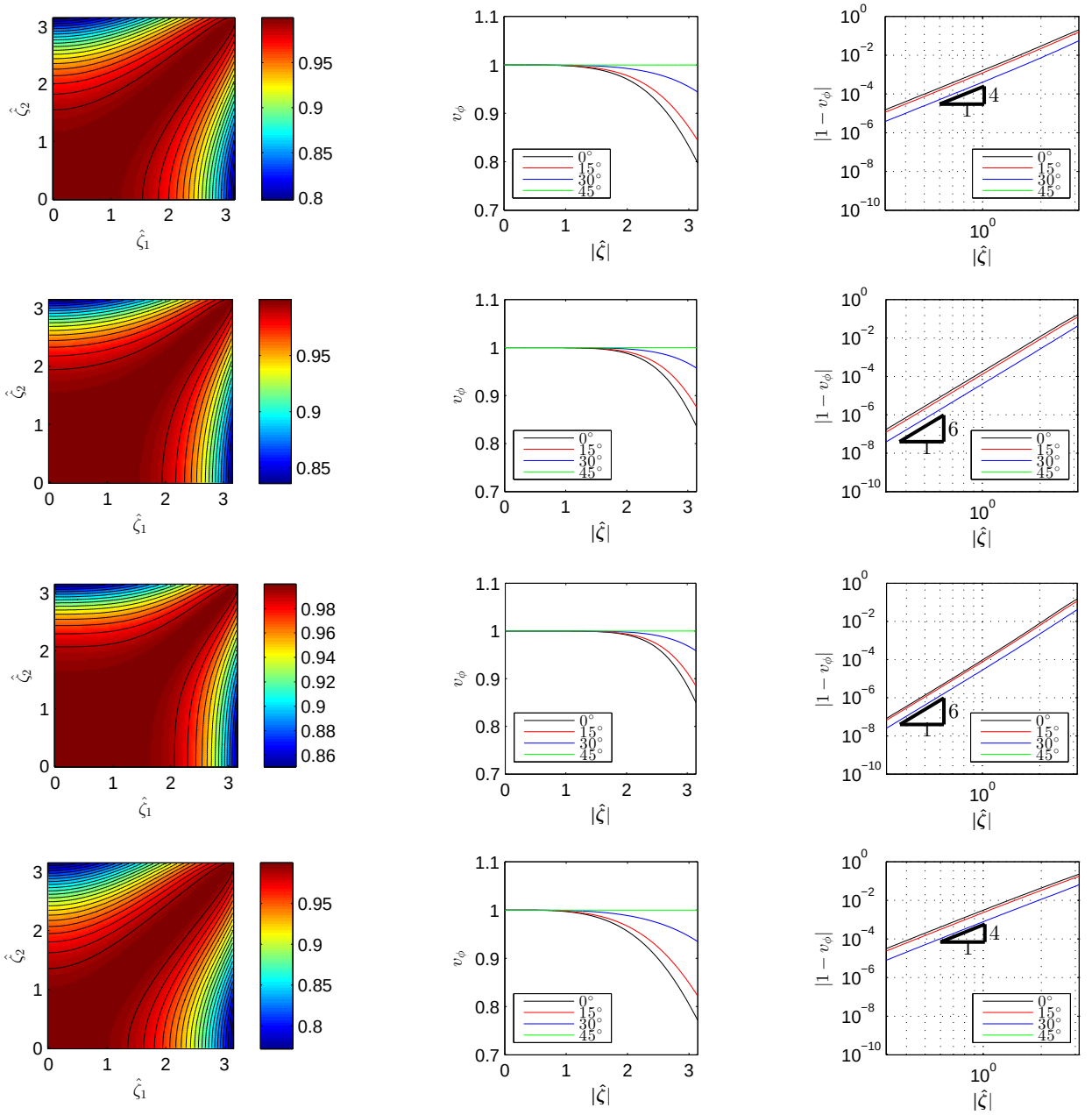

Figure 15: Numerical phase velocity of implicit schemes for the 2D wave equation, for the fourth-order accurate scheme with $N^{(e)} = 2$ and $N^{(i)} = 1$ (top), a sixth-order accurate scheme with $N^{(e)} = N^{(i)} = 3$ (second row), and a sixth-order accurate scheme with $N^{(e)} = 4$ and $N^{(i)} = 2$, (third row) and a fourth-order accurate scheme over a star-shaped stencil (bottom row), with $\lambda = 1/\sqrt{2}$. Left: 1% contours. Middle: as a function of wavenumber, for various angles, as indicated. Right: error as a function of wavenumber magnitude, for various angles, as indicated.

See Figure 16, illustrating the stencils of these families of approximations. Such stencils, herein dubbed "star-shaped", are typically used for their ability to achieve high-order accuracy in space for the Laplacian [17, 31]. In particular, an important known result [31] is that the property (33) is satisfied under the particular choice:

$$\alpha_{M,m} = (-1)^{m-1} \frac{2(M!)^2}{(M-m)!(M+m)!}, \quad m = 1, \ldots, M, \tag{93}$$

with $\boldsymbol{\alpha}^{(e)} = [\alpha_{M,0}, \alpha_{M,1}, \ldots, \alpha_{M,M}]$ and $\mathcal{Q} = \mathcal{S}^{(M)}$.

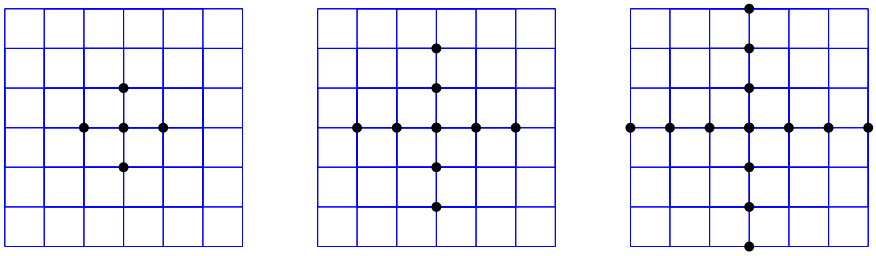

Figure 16: Stencils of approximations to the 2D Laplacian over $\mathcal{S}_2^{(1)}$, $\mathcal{S}_2^{(2)}$ and $\mathcal{S}_2^{(3)}$.

Consider such stencils in explicit schemes for the 2D wave equation, with $\mathcal{Q}^{(e)} = \mathcal{S}_2^{(N^{(e)})}$ and $\mathcal{Q}^{(i)} = \emptyset$.

For Mth order accuracy, the constraints (29) must be satisfied to order $2M$, for the explicit Laplacian operator. Recall, though, that for Laplacians defined over star-shaped stencils, g, as defined in (23), is identically zero for $\boldsymbol{\eta} \in \tilde{\mathbb{M}}^{(m)}$. This implies that $r^{(m)}_{\mathcal{Q}^{(e)},\boldsymbol{\alpha}^{(e)}} = 0$, $m = 2, \ldots, M$. The constraints (49) for higher order accuracy cannot be satisfied under these conditions, and thus such explicit schemes are limited to second-order accuracy, despite their ability to provide high-order approximations to the Laplacian in isolation.

The situation is slightly different for two-step implicit schemes utilising these stencils. Suppose now that $\mathcal{Q}^{(e)} = \mathcal{S}_2^{(N^{(e)})}$ and $\mathcal{Q}^{(i)} = \mathcal{S}_2^{(N^{(i)})}$. As before, for accuracy to $2M$th order, $r^{(m)}_{\mathcal{Q}^{(e)},\boldsymbol{\alpha}^{(e)}} = 0$, $m = 2, \ldots, M$. Furthermore, $r^{(m)}_{\mathcal{Q}^{(i)},\boldsymbol{\alpha}^{(e)}} = 0$, $m = 2, \ldots, M-1$. The conditions for accuracy reduce to

$$\lambda^2 = -w_1^{(m)} r^{(1)}_{\mathcal{Q}^{(i)}} \qquad m = 2, \ldots, M \tag{94}$$

These constraints cannot be simultaneously satisfied beyond $M = 2$, and thus such schemes are at most fourth-order accurate.

As an example of such a fourth-order scheme, consider the case of $\mathcal{Q}^{(e)} = \mathcal{S}_2^{(2)}$ and $\mathcal{Q}^{(i)} = \mathcal{S}_2^{(1)}$. Consistency, isotropy and accuracy conditions to fourth order give the parameter set and stability condition

$$\boldsymbol{\alpha}^{(e)} = \left[\frac{4}{3}, \quad -\frac{1}{3}\right]^{\mathrm{T}} \quad \boldsymbol{\alpha}^{(i)} = \left[-\frac{\lambda^2}{12}\right] \qquad \lambda \leq 1/\sqrt{2} \tag{95}$$

This scheme is novel, and it is worth pointing out that it its stencils reach out to fewer spatial points than a conventional fourth-order accurate theta scheme, which would necessarily employ nine-point stencils in 2D for both explicit and implicit parts. See Figure 15.

5.2.4. Numerical Results

Numerical results are illustrated with an extension of the simple problem formulation used in 1D, as described in Section 5.1.3.

Consider the problem of the 2D wave equation, over the periodic domain $\mathbf{x} \in [-1/2, 1/2)^2$, and with initial data $v_0(\mathbf{x}) = \exp\left(-|\mathbf{x}|^2/2\sigma^2\right)$, and with $v_1(\mathbf{x}) = 0$. The various schemes presented here may be initialised, at the first two time steps, with exact values of the solution, sampled over the grid, obtained through Fourier analysis. For a given duration T, simulated values are generated under refinement of the time step k, assumed to subdivide T evenly; the grid spacing h is set as $h = k/\lambda$, for fixed Courant number λ. If the calculated values are written as $u_{\mathbf{l}}^{(\mathrm{sim})}$, and exact values, obtained from exact values of the solution at time T, again obtained through Fourier analysis, are written as $u_{\mathbf{l}}^{(\mathrm{ex})}$, for $\mathbf{l} \in \mathbb{D}(k)$, where $\mathbb{D}(k)$ is the finite set of grid indices over which the solution is computed for a given time step k, then the relative L^2

error may be written as

$$E(k) = \sqrt{\frac{\sum_{\mathbf{l}\in\mathbb{D}(k)} \left(u_{\mathbf{l}}^{(\mathrm{ex})} - u_{\mathbf{l}}^{(\mathrm{sim})}\right)^2}{\sum_{\mathbf{l}\in\mathbb{D}(k)} \left(u_{\mathbf{l}}^{(\mathrm{ex})}\right)^2}} \tag{96}$$

See Figure 17. Although convergence at the anticipated rate is observed in all cases, there can be a good deal of variation in the error across schemes of a given order of accuracy—as much as an order of magnitude. Furthermore, the convergence rate for a scheme of a given order of accuracy may not be attained until the time step is relatively low—meaning that well-designed schemes of formally lower order of accuracy can outperform such methods, especially taking into consideration the increase in the operation count with the order of accuracy.

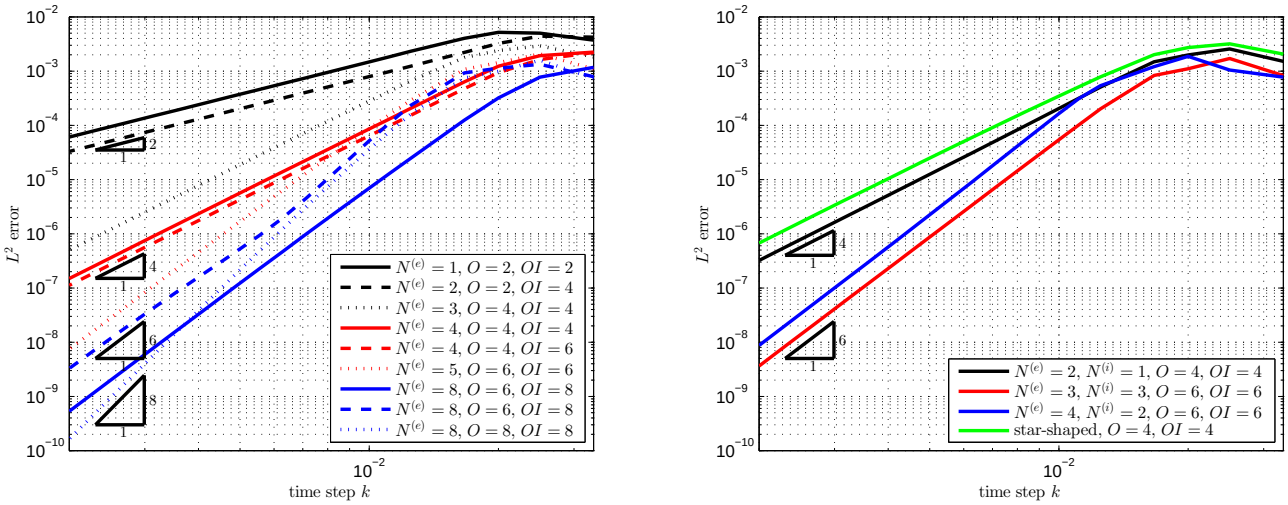

Figure 17: Relative L^2 error $E(k)$, as defined in (96), as a function of k, the time step, on a doubly logarithmic scale, for the test problem as described at the beginning of Section 5.2.4, for $\sigma = 0.0225$, and for $T = 0.1$. Left: for explicit schemes, of order of accuracy O and order of isotropy OI as indicated. Right: for the implicit schemes. In all cases, the Courant number λ is chosen at its maximal value.

As another example, consider the 2D wave equation initialised with the Laplacian of a Gaussian distribution, defined as $v_0(\mathbf{x}) = \left(1 - |\mathbf{x}|^2/2\sigma^2\right) \exp\left(-|\mathbf{x}|^2/2\sigma^2\right)$. For equal memory costs, a fixed choice of grid spacing h is chosen, and plots of the resulting solution after a given duration T are as illustrated in Figure 18.

5.3. 3D

A general approximation to the 3D Laplacian may be written over the set $\mathcal{G}_3^{(N)}$, consisting of the first N admissible 3-vectors.

$$\mathcal{G}_3^{(1)} = \{[1\ 0\ 0]\}, \quad \mathcal{G}_3^{(2)} = \{[1\ 0\ 0], [1\ 1\ 0]\}, \quad \mathcal{G}_3^{(3)} = \{[1\ 0\ 0], [1\ 1\ 0], [2\ 0\ 0]\}, \ldots \tag{97}$$

5.3.1. General Explicit Schemes

When $N^{(e)} = 1$, the simplest possible explicit scheme for the 3D wave equation results [1], sometimes referred to as the seven-point scheme. The stability condition for this scheme is $\lambda \leq 1/\sqrt{3} \approx 0.577$.

When $N^{(e)} = 2$, a well-known 19-point scheme results [53]. Employing a consistency constraint as well as a condition for fourth-order isotropy leads to the system

$$\begin{bmatrix} 1 & 1 \\ 1 & -\frac{1}{2} \end{bmatrix} \begin{bmatrix} \alpha_1^{(e)} \\ \alpha_2^{(e)} \end{bmatrix} = \begin{bmatrix} 1 \\ 0 \end{bmatrix} \qquad \Rightarrow \qquad \boldsymbol{\alpha}^{(e)} = \begin{bmatrix} \frac{1}{3}, & \frac{2}{3} \end{bmatrix}^{\mathrm{T}} \tag{98}$$

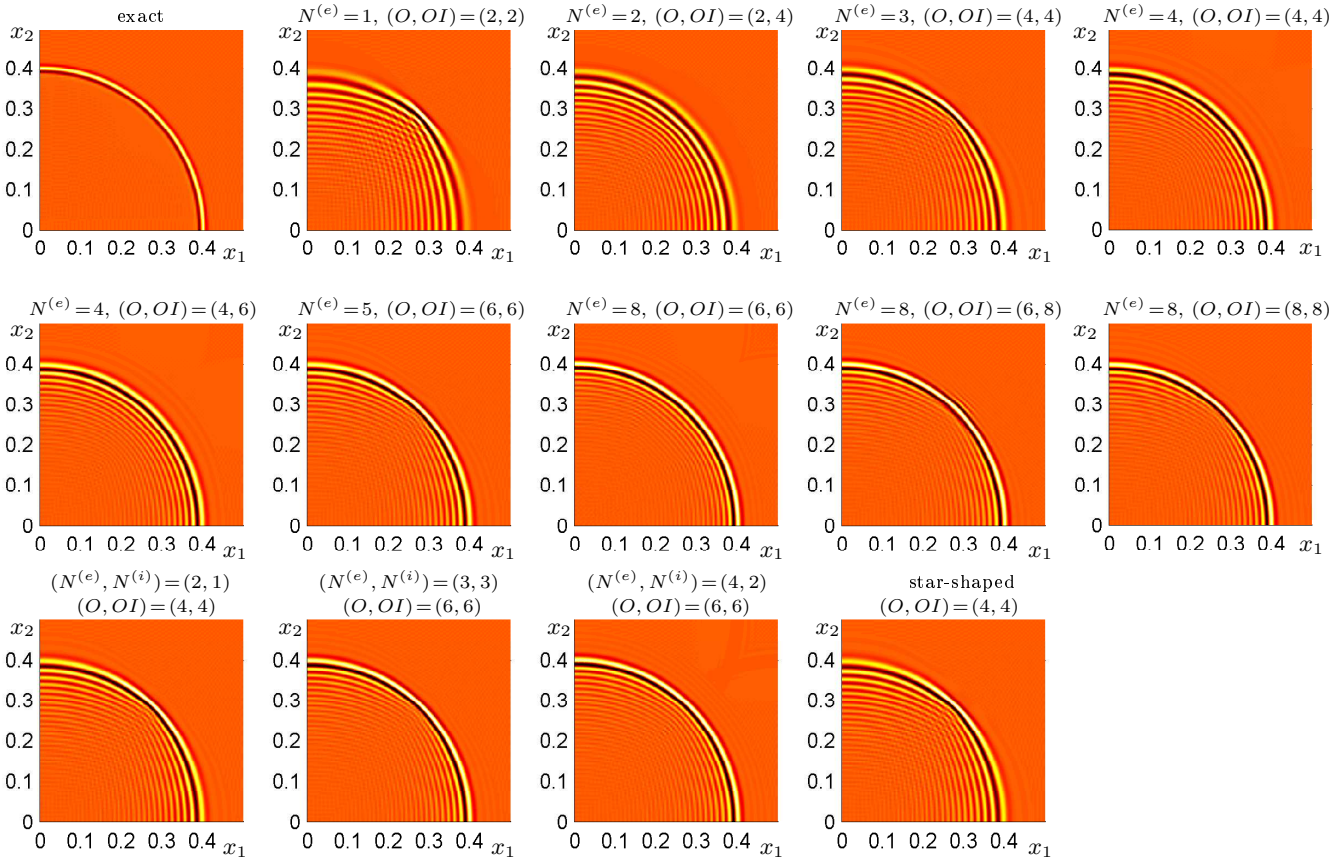

Figure 18: Solution, after the duration $T = 0.4$, using an initial condition of $v_0(\mathbf{x}) = \left(1 - |\mathbf{x}|^2/2\sigma^2\right) \exp\left(-|\mathbf{x}|^2/2\sigma^2\right)$, for $\sigma = 0.005$ for a variety of explicit and implicit schemes with orders of accuracy O and orders of isotropy OI, as indicated, and for a fixed grid spacing of $h = 0.005$. The Courant number λ is chosen at its maximal value in all cases. Note, the "star-shaped" scheme is implicit, allowing it to achieve fourth-order accuracy.

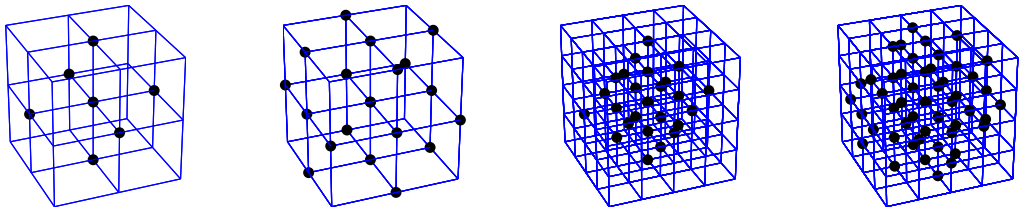

Figure 19: Stencils of approximations to the 3D Laplacian over $\mathcal{G}_3^{(1)}$, $\mathcal{G}_3^{(2)}$, $\mathcal{G}_3^{(3)}$ and $\mathcal{G}_3^{(4)}$.

The stability condition for this scheme may be calculated easily as $\lambda \leq \sqrt{3}/2$.

When $N^{(e)} = 3$, a 25-point scheme results; this is the simplest explicit scheme in 3D for which fourth-order accuracy is possible, and is the second of the 3D diamond-shaped family schemes found in [30] (the first being the simplest scheme). The constraints and coefficients may be written as

$$\begin{bmatrix} 1 & 1 & 1 \\ 1 & -\frac{1}{2} & 4 \\ 1 & 1 & 4 \end{bmatrix} \begin{bmatrix} \alpha_1^{(e)} \\ \alpha_2^{(e)} \\ \alpha_3^{(e)} \end{bmatrix} = \begin{bmatrix} 1 \\ 0 \\ \lambda^2 \end{bmatrix} \qquad \Rightarrow \qquad \boldsymbol{\alpha}^{(e)} = \frac{1}{3}\begin{bmatrix} 4 - 3\lambda^2\,, & 2\lambda^2\,, & \lambda^2 - 1 \end{bmatrix}^{\mathrm{T}} \tag{99}$$

The scheme is stable under the condition $\lambda \leq 1/\sqrt{3}$.

When $N^{(e)} = 5$, one may employ conditions of fourth-order accuracy and sixth-order isotropy to yield a scheme with coefficients

$$\boldsymbol{\alpha}^{(e)} = \left[\frac{2}{15} + \frac{1}{9}\lambda^2\,, \quad \frac{8}{5} - \frac{8}{9}\lambda^2\,, \quad \frac{1}{5} - \frac{1}{9}\lambda^2\,, \quad -\frac{4}{15} + \frac{1}{3}\lambda^2\,, \quad -\frac{2}{3} + \frac{5}{9}\lambda^2\right]^{\mathrm{T}} \tag{100}$$

This scheme, which also appears in [54], is stable under the conditions $\sqrt{4/15} \leq \lambda \leq \sqrt{\frac{3}{10}(6-\sqrt{11})} \approx 0.896$. Note in particular the appearance of a lower bound on the Courant number—the first such instance in this study; this lower bound results from condition (55a), which has thus far been satisfied without additional constraints on λ. This scheme has the advantage of a Courant number more than 50% higher than the 25-point diamond scheme.

When $N^{(e)} = 6$, a sixth-order accurate scheme, diamond-shaped, may be obtained, with coefficients

$$\boldsymbol{\alpha}^{(e)} = \left[\frac{3}{2} - \frac{115}{72}\lambda^2 + \frac{41}{120}\lambda^4\,, \quad \frac{10}{9}\lambda^2 - \frac{2}{5}\lambda^4\,, \quad -\frac{3}{5} + \frac{8}{9}\lambda^2 - \frac{1}{5}\lambda^4\,, \quad \frac{1}{15}\lambda^4\,, \quad -\frac{5}{18}\lambda^2 + \frac{1}{6}\lambda^4\,, \quad \frac{1}{10} - \frac{1}{8}\lambda^2 + \frac{1}{40}\lambda^4\right]^{\mathrm{T}} \tag{101}$$

The scheme is stable under the condition $\lambda \leq 1/\sqrt{3}$ [30]. See Figure 20.

5.3.2. Implicit Schemes

The simplest implicit scheme of fourth-order accuracy for the 3D wave equation can be constructed using $N^{(e)} = 2$ and $N^{(i)} = 1$. It has coefficients

$$\boldsymbol{\alpha}^{(e)} = \left[\frac{1}{3}\,, \quad \frac{2}{3}\right]^{\mathrm{T}} \qquad\qquad \alpha_1^{(i)} = \frac{1-\lambda^2}{12} \tag{102}$$

This novel scheme, which can be seen as the 3D analogue of the 2D scheme given by (87), is stable under the condition $\lambda \leq 1/\sqrt{2}$.

Going further, a novel sixth-order accurate scheme may be constructed using $N^{(e)} = 4$ and $N^{(i)} = 3$. It has coefficients

$$\boldsymbol{\alpha}^{(e)} = \left[\frac{4}{15}\,, \quad \frac{8}{15}\,, \quad \frac{1}{15}\,, \quad \frac{2}{15}\right]^{\mathrm{T}} \quad \boldsymbol{\alpha}^{(i)} = \left[\frac{1}{15} - \frac{1}{90}\lambda^2 - \frac{1}{20}\lambda^4\,, \quad \frac{2}{45} - \frac{1}{15}\lambda^2 + \frac{1}{30}\lambda^4\,, \quad -\frac{1}{90} - \frac{1}{180}\lambda^2 + \frac{1}{60}\lambda^4\right]^{\mathrm{T}} \tag{103}$$

The scheme is stable under the condition $\lambda \leq 1/\sqrt{3}$. See Figure 21.

5.3.3. Numerical Results

Numerical results are illustrated with an extension of the simple problem formulation used in 1D and 2D, as described in Sections 5.1.3 and 5.2.4.

Similarly to the case of 2D, consider the problem of the 3D wave equation, over the periodic domain $\mathbf{x} \in [-1/2, 1/2)^3$, and with initial data $v_0(\mathbf{x}) = \exp\left(-|\mathbf{x}|^2/2\sigma^2\right)$, and with $v_1(\mathbf{x}) = 0$. Initialization values and the exact solution are again obtained through Fourier analysis. See Figure 22, illustrating convergence at anticipated rates for all cases.

6. Concluding Remarks

A general framework for the construction of high-order accurate two-step implicit/explicit schemes for the wave equation in d spatial dimensions has been presented in this paper. The construction relies on a delicate balance of spatial and temporal errors achieved through modified equation representations of the schemes and careful selection of parameters through linear constraints imposed for high orders of isotropy, and nonlinear constraints in the case of higher order accuracy. Various high-order two-step schemes that have appeared previously in the literature are found as special cases of this general construction, and multiple novel special cases have been presented, of both explicit and implicit type. The benefits of this framework include: flexibility in choosing stencil shapes and sizes, without relying on the use of recursive

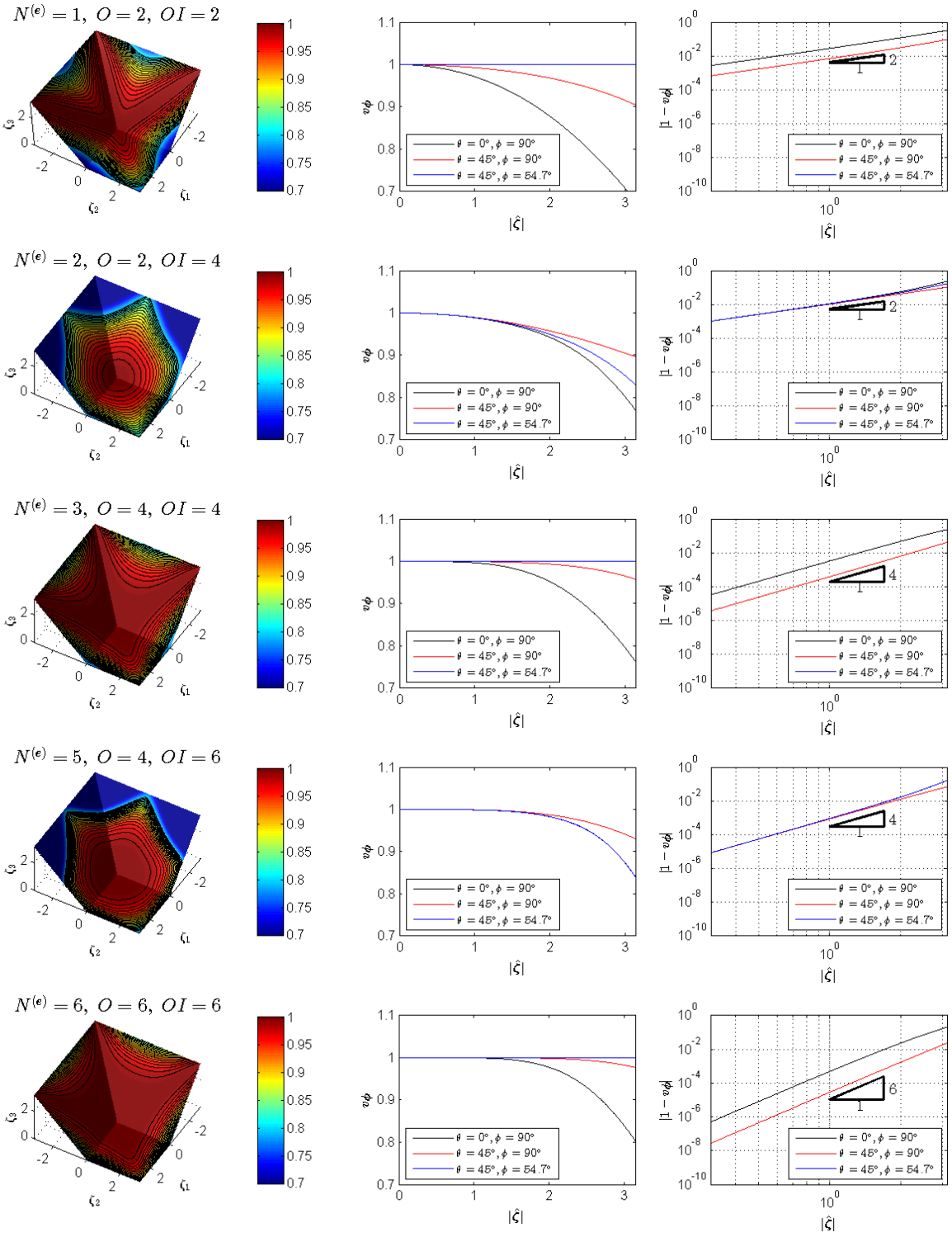

Figure 20: Numerical phase velocity of the explicit schemes for the 3D wave equation, with $N^{(e)}$, the order of accuracy O and order of isotropy OI as indicated. The Courant number λ is taken at its maximal value in all cases. Left: 1% contours. Middle: as a function of wavenumber, for various angle pairs θ, ϕ, as indicated. Right: error as a function of wavenumber, for various angle pairs, as indicated.

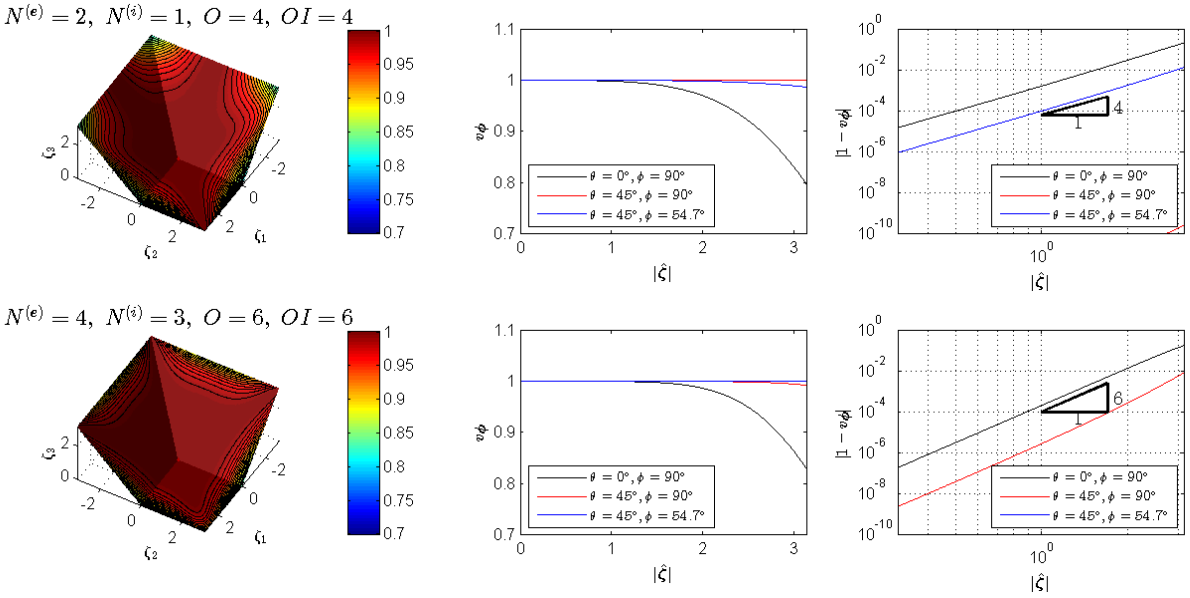

Figure 21: Numerical phase velocity of implicit schemes for the 3D wave equation, with $N^{(e)}$, $N^{(i)}$, the order of accuracy O and order of isotropy OI as indicated. The Courant number λ is taken at its maximal value in all cases. Left: 1% contours. Middle: as a function of wavenumber, for various angle pairs θ, ϕ, as indicated. Right: error as a function of wavenumber, for various angle pairs, as indicated.

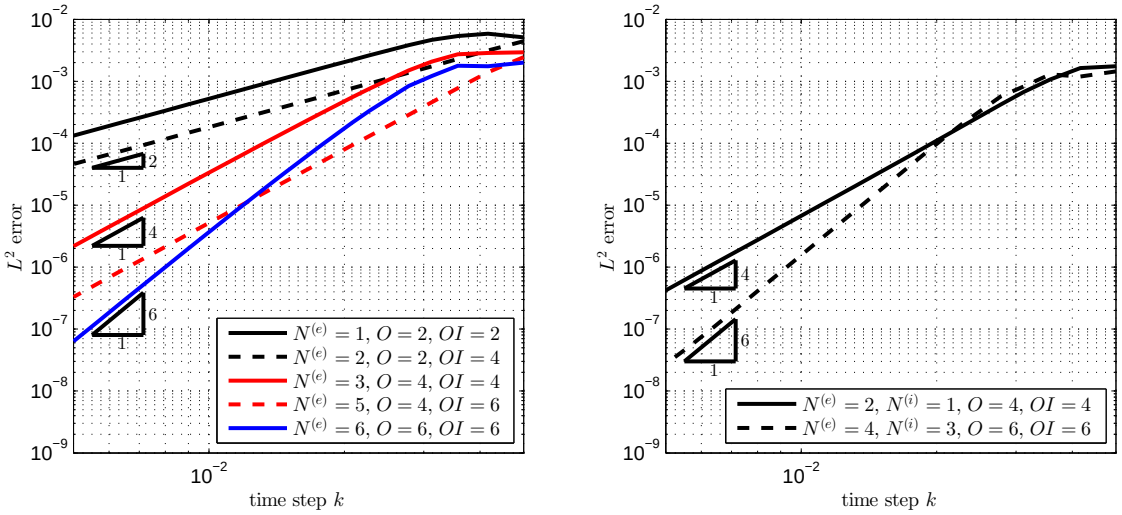

Figure 22: Relative L^2 error $E(k)$, as defined in (96), as a function of k, the time step, on a doubly logarithmic scale, for the test problem as described at the beginning of Section 5.2.4, for $\sigma = 0.01$, and $T = 0.25$. Left: for explicit schemes, of order of accuracy O and order of isotropy OI as indicated. Right: for the implicit schemes. In all cases, the Courant number λ is chosen at its maximal value.

scheme generation strategies, and allowing for a good degree of control over computational cost, particularly for explicit schemes; the relatively independent specification of orders of isotropy and accuracy; and the possibility of constructing schemes with Courant numbers close to unity, surpassing high-order two-step schemes in the literature that are typically limited to the standard CFL condition. It is interesting to note that among the members of the very general family of schemes presented here, none has been found which permits a Courant number larger than unity.

A major concern not addressed here is that of suitable boundary termination for such schemes. This is obviously complicated by the use of wide-reaching stencils (with multiple *ghost points* falling outside of the

domain), and there will be additional concerns for maintaining high orders of accuracy for the combined initial-boundary value problem. However, it should be remembered that despite these challenges, they are less severe than those found in spectral methods, where underlying stencils are infinite in size [15]; therein lies the potential advantage of the construction framework presented in this paper—the flexibility to choose stencil shape and size and trade-off of accuracy for ease in grid truncation. There are various avenues from which one could approach the associated boundary problem. Appropriate summation-by-parts matrix norms could, in theory, be derived for such stencils, and penalty techniques, as used in the highly successful SBP-SAT approach [22], could also be employed here. Alternatively, one could follow the approach taken by Henshaw, where suitable electromagnetic boundary truncation is successfully applied to high-order schemes (derived using similar modified equation methods) for Maxwell's equations [23]. Hybridizations of spectral methods with other lower-order, more compact approaches have been presented in [55], and similar techniques could be used in the context of these schemes. Absorbing boundary conditions for wave equations could be reasonably be treated using the principle of images [56], or via absorbing layers, as in [57]. On the other hand, construction of perfectly matched layers (PMLs) may present significant challenges for some of these schemes, although some possible strategies the subfamily of 2D diamond-shaped schemes are discussed in [8].

For a given choice of stencil, the conditions for isotropy, accuracy and stability given in this article are framed as a set of coupled constraints on the scheme parameters as well as the Courant number. Such constraints could be used as the starting point for optimization procedures if the number of scheme parameters is larger than the number of constraints. The error measure will almost certainly depend on the deviation of the wave speed from the ideal value of 1 over some range of wavenumbers, and one could envisage trading off order of accuracy or isotropy for decreased error over a wide range of wavenumbers. There are various difficulties which emerge. First is the question of the solution space. Conditions under which the constraints taken together admit a space of possible solutions are not evident; a trivial case described here is that of the family of schemes over star-shaped stencils, for which accuracy to order greater than two is ruled out. Second is the question of the choice of cost function, which clearly must take into account various factors, including a) the number of operations required at a given grid point in order to evaluate a discrete Laplacian, b) the time/space grid density, which will be influenced by the choice of the Courant number, c) the operation count associated with linear system solutions in the case of an implicit method, and d) the range of wavenumbers over which to optimize, the form of error measure (such as L_2 or L_∞) and whether to employ a weighting function of some kind. Third, given a choice of cost function, is the question of whether the complete optimisation problem, consisting of the cost function as well as the various constraints is tractable (i.e., does it possess desirable attributes such as smoothness or convexity?). Still, it would seem to be a useful way to proceed, particularly if one is interested in achieving good performance of a scheme over a wide range of wavenumbers.

7. Acknowledgment

This work was supported by the European Research Council, under grants ERC-StG-2011-279068-NESS and ERC-PoC-2016-737574-WRAM. Thanks to Shyam Prabhakar of the Genome Institute of Singapore for many interesting discussions regarding the cardinality of $\tilde{\mathbb{M}}^{(m)}$.

Appendix A. Discrete Energy Conservation

Though frequency domain techniques have been employed here for analysis purposes, it is useful to note that the schemes presented here do exhibit a discrete energy conservation property. Energy methods applied to the case of discrete schemes for the wave equation have been employed by many authors, usually in the interest of determining suitable boundary conditions [22, 57].

For the sake of simplicity, consider an explicit scheme of the form (40) in d dimensions, including a single Laplacian approximation, characterised by an admissible d-vector $\mathbf{q}$. The scheme then reduces to

$$\delta_{tt} u_{\mathbf{l}}^n = \delta_{\mathbf{q}} u_{\mathbf{l}}^n \,, \tag{A.1}$$

where $\delta_{\mathbf{q}}$ is as defined in (11). As a first step, it is useful to rewrite the averaging operator $\mu_\nu^{(b)}$, for integer $\nu = 1, \ldots, d$, and for integer $b \geq 0$, as defined in (10), as

$$\mu_\nu^{(b)} = 1 + \frac{h^2}{2}\delta_{\nu\nu}^{(b)} \qquad \delta_{\nu\nu}^{(b)} = \frac{1}{b^2h^2}\left(e_{\nu+}^b - 2 + e_{\nu-}^b\right), \tag{A.2}$$

and note that $\delta_{\nu\nu}^{(0)} = 0$. It then follows that $\delta_{\mathbf{q}}$ may be rewritten in terms of a weighted sum of products of operators of the form $\delta_{\nu\nu}^{(b)}$ as

$$\delta_{\mathbf{q}} = \sum_{\mathbf{j}\in\mathbb{Z}^d} \Omega_{\mathbf{q}}^{(\mathbf{j})} \prod_{\nu=1}^{d} \delta_{\nu\nu}^{(j_\nu)}, \tag{A.3}$$

where $\Omega_{\mathbf{q}}^{(\mathbf{j})}$ are weighting coefficients which depend on $\mathbf{q}$ as well as h, and are indexed by the integer-values d-vector $\mathbf{j} = [j_1, \ldots, j_d]$.

We may also define the forward, backward and centered time difference operators δ_{t+}, δ_{t-} and $\delta_{t\circ}$ by

$$\delta_{t+} = \frac{1}{k}\left(e_{t+} - 1\right) \qquad \delta_{t-} = \frac{1}{k}\left(1 - e_{t-}\right) \qquad \delta_{t\circ} = \frac{1}{2k}\left(e_{t+} - e_{t-}\right) \tag{A.4}$$

and forward and backward b-step spatial difference operators by

$$\delta_{\nu+}^{(b)} = \frac{1}{bh}\left(e_{\nu+}^b - 1\right) \qquad \delta_{\nu-}^{(b)} = \frac{1}{bh}\left(1 - e_{\nu-}^b\right). \tag{A.5}$$

Note that

$$\delta_{\nu\nu}^{(b)} = \delta_{\nu+}^{(b)}\delta_{\nu-}^{(b)} \tag{A.6}$$

referring to the operator $\delta_{\nu\nu}^{(b)}$ defined in (A.2).

Now, define the usual l_2 inner product and norm over $\mathbb{Z}^d$ as

$$\langle f^n, g^n\rangle = h^d \sum_{\mathbf{l}\in\mathbb{Z}^d} f_{\mathbf{l}}^n g_{\mathbf{l}}^n \qquad \|f\| = \sqrt{\langle f^n, f^n\rangle} \tag{A.7}$$

for grid functions $f_{\mathbf{l}}^n$ and $g_{\mathbf{l}}^n$, $l \in \mathbb{Z}^d$. The following identities hold [58]:

$$\langle \delta_{t\circ} f^n, \delta_{tt} f^n\rangle = \delta_{t+}\left(\frac{1}{2}\|\delta_{t-} f^n\|^2\right) \qquad \langle \delta_{t\circ} f^n, f^n\rangle = \delta_{t+}\left(\frac{1}{2}\langle f^n, e_{t-} f^n\rangle\right), \tag{A.8}$$

$$\langle f^n, \delta_{\nu\nu}^{(b)} g^n\rangle = \langle f^n, \delta_{\nu+}^{(b)}\delta_{\nu-}^{(b)} g^n\rangle = -\langle \delta_{\nu-}^{(b)} f^n, \delta_{\nu-}^{(b)} g^n\rangle. \tag{A.9}$$

Taking the inner product of (A.1) with $\delta_{t\circ} u_{\mathbf{l}}^n$ leads to

$$\langle \delta_{t\circ} u^n, \delta_{tt} u^n\rangle = \langle \delta_{t\circ} u^n, \delta_{\mathbf{q}} u^n\rangle. \tag{A.10}$$

The left hand side may be rewritten, using the first of the identities in (A.8), as

$$\delta_{t+}\mathfrak{t}^n \qquad \text{where} \qquad \mathfrak{t}^n = \frac{1}{2}\|\delta_{t-} u^n\|^2. \tag{A.11}$$

The right hand side may be rewritten, using the second of the identities in (A.8), and (A.9), as

$$-\delta_{t+}\mathfrak{v}_{\mathbf{q}}^n \qquad \text{where} \qquad \mathfrak{v}_{\mathbf{q}}^n = \frac{1}{2}\sum_{\mathbf{j}\in\mathbb{Z}^d} \Omega_{\mathbf{q}}^{(\mathbf{j})} \langle \prod_{\nu=1}^{d} \delta_{\nu-}^{(j_\nu)} u^n, e_{t-} \prod_{\nu=1}^{d} \delta_{\nu-}^{(j_\nu)} u^n\rangle. \tag{A.12}$$

Defining $\mathfrak{e}^n$ as $\mathfrak{e}^n = \mathfrak{t}^n + \mathfrak{v}_{\mathbf{q}}^n$, leads to

$$\delta_{t+}\mathfrak{e}^n = 0 \qquad \text{or} \qquad \mathfrak{e}^n = \text{constant}. \tag{A.13}$$

There is thus a conserved quantity associated with this scheme which may be viewed as a discrete energy. It is not, however, a non-negative function of the state, and thus cannot be used directly in order to show

stability of the scheme unless an additional condition for non-negativity is also determined. Normally, this condition will be expressed as an upper bound on λ ,the Courant number.

The construction above extends in a natural way to schemes with parameterised Laplacian approximations such as (40). For example, for an explicit parameterised scheme, with index set $\mathcal{Q}^{(e)} = \{\mathbf{q}_1, \ldots, \mathbf{q}_{N^{(e)}}\}$ and associated parameters $\boldsymbol{\alpha} = [\alpha_1, \ldots, \alpha_{N^{(e)}}]^{\mathrm{T}}$, the conserved energetic quantity follows directly from linearity as

$$\mathfrak{e}^n = \mathfrak{t}^n + \sum_{p=1}^{N^{(e)}} \alpha_p \mathfrak{v}^n_{\mathbf{q}_p} \,, \tag{A.14}$$

and, as in the case of the scheme with a single Laplacian approximation, non-negativity conditions must be found in order to determine a stability condition.

Appendix B. Conditions for Negativity of Laplacian Operators

The condition (55a), necessary for stability for the scheme (40), is a natural condition on negativity (or, more properly, non-positivity) of an approximation $\hat{\delta}_{\mathcal{Q},\boldsymbol{\alpha}}$ to the Laplacian, defined over some index set $\mathcal{Q} = \{\mathbf{q}_1, \ldots, \mathbf{q}_N\}$, as in (14), and with coefficients $\boldsymbol{\alpha} = [\alpha_1, \ldots, \alpha_N]$. Here, the coefficients $\boldsymbol{\alpha}$ satisfy the condition (15), so that $\hat{\delta}_{\mathcal{Q},\boldsymbol{\alpha}}$ is indeed a consistent approximation to the Laplacian.

It is equivalent to consider either the negativity of the operator in the spatial domain, i.e.,

$$\langle f, \hat{\delta}_{\mathcal{Q},\boldsymbol{\alpha}} f \rangle \leq 0 \,, \tag{B.1}$$

for any grid function $f_{\mathbf{l}}$ defined for $\mathbf{l} \in \mathbb{Z}^d$, or in the wavenumber domain:

$$\hat{D}_{\mathcal{Q},\boldsymbol{\alpha}}(\boldsymbol{\zeta}) \leq 0 \qquad \text{for} \qquad \boldsymbol{\zeta} \in \mathbb{U}^d \,, \tag{B.2}$$

where $\hat{D}_{\mathcal{Q},\boldsymbol{\alpha}}(\boldsymbol{\zeta})$ is the scaled spatial Fourier transform of the operator $\hat{\delta}_{\mathcal{Q},\boldsymbol{\alpha}}$, as defined in (39).

In general, finding necessary and sufficient conditions for the negativity of an operator such as $\hat{D}_{\mathcal{Q},\boldsymbol{\alpha}}(\boldsymbol{\zeta})$ reduces, ultimately, to the problem of the analysis of the negativity of multivariate polynomials. Indeed, from (38), the Fourier transform $D_{\mathbf{q}}(\boldsymbol{\zeta})$ of any Laplacian approximation $\delta_{\mathbf{q}}$ defined over a given shell indexed by $\mathbf{q}$ can be written as a polynomial in the functions $c^{(1)}_\nu = \cos(\zeta_\nu h)$, $\nu = 1, \ldots, d$, and thus the transform of any parameterised Laplacian such as $\hat{D}_{\mathcal{Q},\boldsymbol{\alpha}}(\boldsymbol{\zeta})$ may be as well. Simple conditions for negativity are not forthcoming—the study of negative (positive) polynomials is a longstanding research area—see [59] for a review. In this short appendix, some simple conditions for negativity are provided.

Appendix B.1. Positivity of Coefficients

Sufficient conditions restricting the range of possible Laplacian approximations are available. In the present setting of Laplacian approximations defined over shells, for which the Fourier transforms are as given in (38), it may be remarked that any individual such approximation, for a given shell $\mathbf{q}$ is necessarily negative. This follows from the observation that because $c^{(b)}_\nu = \cos(\zeta_\nu b h)$ is bounded in magnitude by 1, each term in the sum in (38) is negative. It thus follows that for the Fourier transform $D_{\mathcal{Q},\boldsymbol{\alpha}}(\boldsymbol{\zeta})$ of any parameterised Laplacian $\hat{\delta}_{\mathcal{Q},\boldsymbol{\alpha}}$, the condition

$$\alpha_p \geq 0 \qquad p = 1, \ldots, N \qquad \rightarrow \qquad D_{\mathcal{Q},\boldsymbol{\alpha}}(\boldsymbol{\zeta}) \leq 0 \tag{B.3}$$

must hold. This condition could be used as an additional constraint in the design of the schemes presented in this article, and thus condition (55a) is satisfied automatically. It is clear, though, that this condition is sufficient but not necessary—and indeed rules out at least some (if not all) higher-order accurate designs. See the example given in Appendix B.3 below.

Appendix B.2. Decompositions of the Laplacian

A more interesting family of conditions results from the decomposition of the Laplacian approximation into operator pairs, as per the decomposition of the Laplacian as $\Delta = (\nabla\cdot)\,\nabla$, where ∇ is a d-dimensional gradient operation, and where $\nabla\cdot$ is the d-dimensional divergence.

In order to construct such operators, it is useful to begin by defining forward and backward spatial difference and averaging operators in dimension ν, $\nu = 1, \ldots, d$. Basic one-step difference operators may be defined, with reference to the more general difference operators defined in (A.5), as

$$\delta_{\nu+} \triangleq \delta^{(1)}_{\nu+} = \frac{1}{h}\,(e_{\nu+} - 1) \qquad \delta_{\nu-} \triangleq \delta^{(1)}_{\nu-} = \frac{1}{h}\,(1 - e_{\nu-})\;, \tag{B.4}$$

and averaging operators as

$$\mu_{\nu+} = \frac{1}{2}\,(e_{\nu+} + 1) \qquad \mu_{\nu-} = \frac{1}{2}\,(1 + e_{\nu-})\;. \tag{B.5}$$

Under a d-dimensional inner product, as defined in (A.7), such difference and averaging operators satisfy the following identities:

$$\langle f, \delta_{\nu+} g\rangle = -\langle \delta_{\nu-} f, g\rangle \qquad \langle f, \mu_{\nu+} g\rangle = \langle \mu_{\nu-} f, g\rangle\,. \tag{B.6}$$

A basic approximation to the gradient and divergence, in d dimensions, may then be defined as

$$\nabla = [\delta_{1+}, \ldots, \delta_{d+}]^T \qquad \nabla^\dagger = [\delta_{1-}, \ldots, \delta_{d-}]\,, \tag{B.7}$$

where ∇ and $\nabla^\dagger$ are represented here as column and row d-vectors, respectively, and are negative adjoints due to the property (B.6) above—that is, for any column d-vector grid function $\mathbf{f_l}$ and scalar grid function $g_\mathbf{l}$,

$$\langle \mathbf{f}, \nabla g\rangle = -\langle \nabla^\dagger \mathbf{f}, g\rangle\,. \tag{B.8}$$

An approximation to the Laplacian follows as

$$\hat{\delta} = \nabla^\dagger \nabla\,. \tag{B.9}$$

Note that due to the property (B.8) of the ∇ and $\nabla^\dagger$, it follows that for a Laplacian approximation so defined, for any grid function $f_\mathbf{l}$, with $\mathbf{l} \in \mathbb{Z}$,

$$\langle f, \hat{\delta} f\rangle = \langle f, \nabla^\dagger \nabla f\rangle = -\langle \nabla f, \nabla f\rangle = -\|\nabla f\|^2 \le 0\,, \tag{B.10}$$

and the Laplacian approximation is thus negative by construction. This particular approximation to the the Laplacian corresponds to the simplest variety defined over the first shell $\mathcal{G}^{(1)}_d$ in any dimension d.

Other Laplacian approximations, also negative, may be formed using such negative-adjoint gradient and divergence pairs which include further averaging operations, as defined in (B.5). For example, in 2D, the operator pair

$$\nabla = [\mu_{2+}\delta_{1+}, \mu_{1+}\delta_{2+}]^T \qquad \nabla^\dagger = [\mu_{2-}\delta_{1-}, \mu_{1-}\delta_{2-}]^T \tag{B.11}$$

yields a Laplacian approximation $\delta_{[1\,1]}$ over the shell $\mathbf{q} = [1\ 1]$, and

$$\nabla = [\mu_{1+}\delta_{1+}, \mu_{2+}\delta_{2+}]^T \qquad \nabla^\dagger = [\mu_{1-}\delta_{1-}, \mu_{2-}\delta_{2-}]^T \tag{B.12}$$

gives a Laplacian approximation $\delta_{[2\,0]}$ over the shell $\mathbf{q} = [2\ 0]$.

It follows that a Laplacian approximation built from a weighted positive sum of such factorizable Laplacian approximations is also negative. Suppose that ∇_p, $p = 1 \ldots, P$ are P approximations to the gradient, and $\nabla^\dagger_p$ are their negative adjoints. Then, for any set of parameters $\beta_p \ge 0$, $p = 1, \ldots, P$, with $\sum_{p=1}^P \beta_p = 1$,

$$\hat{\delta} = \sum_{p=1}^{P} \beta_p \nabla^\dagger_p \nabla_p \le 0 \tag{B.13}$$

is an approximation to the Laplacian which is negative by construction.

Appendix B.3. Example

Consider, as a simple but nontrivial example, a 2D Laplacian approximation $\hat{\delta}_{\mathcal{Q},\boldsymbol{\alpha}}$, defined over $\mathcal{Q} = \mathcal{G}_2^{(3)}$, or using the first three shells, and which may be written as

$$\hat{\delta}_{\mathcal{Q},\boldsymbol{\alpha}} = (1 - \alpha_2 - \alpha_3)\, \delta_{[1\,0]} + \alpha_2 \delta_{[1\,1]} + \alpha_3 \delta_{[2\,0]}\,, \tag{B.14}$$

where the constraint (15) has been employed. The conditions for negativity of this operator may be easily computed (from, e.g., the Fourier transform) as

$$\alpha_3 \leq 1 \qquad \alpha_2 + \alpha_3 \leq 1\,. \tag{B.15}$$

Enforcing the positivity condition on the coefficients of the individual Laplacian approximations, however, leads to the sufficient conditions

$$\alpha_2 \geq 0 \qquad \alpha_3 \geq 0 \qquad \alpha_2 + \alpha_3 \leq 1 \tag{B.16}$$

which are more restrictive than the correct conditions (B.15). Indeed, such positivity conditions on the Laplacian coefficients do not permit the construction of the fourth-order accurate explicit scheme for the wave equation given in (80).

In contrast, consider the following approximation to the Laplacian:

$$\hat{\delta} = \frac{1}{2}\nabla_1^\dagger \nabla_1 + \frac{1}{2}\nabla_2^\dagger \nabla_2\,, \tag{B.17}$$

where

$$\nabla_1 = \begin{bmatrix} ((1-\theta-\phi) + \theta\mu_{1+} + \phi\mu_{2+})\,\delta_{1+} \\ ((1-\theta-\phi) + \theta\mu_{2+} + \phi\mu_{1+})\,\delta_{2+} \end{bmatrix} \qquad \nabla_2 = \begin{bmatrix} ((1-\theta+\phi) - \phi\mu_{1+} + \theta\mu_{2+})\,\delta_{1+} \\ ((1-\theta+\phi) - \phi\mu_{2+} + \theta\mu_{1+})\,\delta_{2+} \end{bmatrix} \tag{B.18}$$

are two approximations to the 2D gradient operation, and where $\nabla_1^\dagger$ and $\nabla_2^\dagger$ are the corresponding negative adjoints or divergence operations. The approximation (B.17) is negative by construction, and dependent on two free parameters θ and ϕ, which are unconstrained. But (B.17) may be rewritten, in terms of a combination of Laplacian operations over the first three shells, as

$$\hat{\delta} = \left((1-\theta)^2 + \phi^2\right)\delta_{[1\,0]} + \left(-\frac{1}{2}\theta^2 - \frac{1}{2}\phi^2 + \theta - \phi\right)\delta_{[1\,1]} + \left(-\frac{1}{2}\theta^2 - \frac{1}{2}\phi^2 + \theta + \phi\right)\delta_{[2\,0]}\,, \tag{B.19}$$

which is equivalent to (B.14), under a distinct parametrisation (in θ and ϕ, rather than α_2 and α_3). It may be easily verified that the complete range of parameters θ and ϕ recovers exactly the range of α_2 and α_3 required for negativity as per condition (B.15).

It is conjectured here that any negative Laplacian approximation can be formulated in terms of a positively weighted sum of gradient/divergence approximation pairs, as per (B.13) above.

Appendix B.4. Perspectives

If the conjecture above is true, it then implies that one may work with an equivalent parameterised Laplacian approximation which is negative by construction, then one of the two stability conditions (55a) is satisfied *a priori*; this simplifies the analysis of stability for any of the family of schemes (40) to that of satisfying the second condition (55b). Notice, however, that, even for the simple example given in the previous section, the free parameters (in this case θ and ϕ rather than α_2 and α_3) appear nonlinearly in the final form of the Laplacian approximation, as given in (B.19). This complicates the formulation of the constraints for higher-order accuracy—note that a simple representation of these constraints, such as that given in the case of a parameterisation in terms of shells in (69) is not available.

Appendix C. Theta schemes

Theta schemes [34] on regular Cartesian grids can be seen as a subset of the general family of implicit schemes given by (40). In order to see this, it will help to define the following temporal averaging operator:

$$\mu_{t,\Theta} = \Theta e_{t+} + (1 - 2\Theta) + \Theta e_{t-} = 1 + O(k^2)\,, \tag{C.1}$$

where $\Theta \in \mathbb{R}$ is a free parameter. $\mu_{t,\Theta}$ also has the following relation to δ_{tt} [34]:

$$\mu_{t,\Theta} = 1 + \Theta k^2 \delta_{tt}\,. \tag{C.2}$$

Then, if we reduce the scheme to include only one Laplacian by choosing $\mathcal{Q}^{(i)} = \mathcal{Q}^{(e)} = \mathcal{Q}$ and $\boldsymbol{\alpha}^{(i)} = \lambda^2\Theta\boldsymbol{\alpha}^{(e)} = \lambda^2\Theta\boldsymbol{\alpha}$, the scheme operator $\mathfrak{l}$ in (40) may be rewritten as:

$$\mathfrak{l} = \delta_{tt} - \mu_{t,\Theta}\hat{\delta}_{\mathcal{Q},\boldsymbol{\alpha}}\,. \tag{C.3}$$

which is in the form of so-called "theta schemes".

References

[1] G. E. Forsythe, W. R. Wasow, Finite-difference Methods for Partial Differential Equations, New York: Wiley, 1960.
[2] B. Gustafsson, High Order Difference Methods for Time Dependent PDE, Vol. 38, Springer, 2007.
[3] O. C. Zienkiewicz, R. L. Taylor, The Finite Element Method, Vol. 3, McGraw-Hill London, 1977.
[4] G. Cohen, S. Pernet, Finite Elements and Discontinuous Galerkin Methods for Transient Wave Equations, Springer, 2017.
[5] R. J. LeVeque, Finite Volume Methods for Hyperbolic Problems, Vol. 31, Cambridge University Press, 2002.
[6] B. Fornberg, A Practical Guide to Pseudospectral Methods, Vol. 1, Cambridge University Press, 1998.
[7] R. Courant, K. Friedrichs, H. Lewy, Über die partiellen differenzengleichungen der mathematischen physik, Mathematische Annalen 100 (1) (1928) 32–74.
[8] Y. Liu, M. K. Sen, Time–space domain dispersion-relation-based finite-difference method with arbitrary even-order accuracy for the 2D acoustic wave equation, Journal of Computational Physics 232 (1) (2013) 327–345.
[9] T. H. Pulliam, D. W. Zingg, Fundamental Algorithms in Computational Fluid Dynamics, Springer, 2014.
[10] V. Linders, J. Nordström, Uniformly best wavenumber approximations by spatial central difference operators, Journal of Computational Physics 300 (2015) 695–709.
[11] Y. An, Uniform dispersion reduction schemes for the one dimensional wave equation in isotropic media, Journal of Computational Physics 341 (2017) 13–21.
[12] P. Micikevicius, 3D finite difference computation on GPUs using CUDA, in: Proceedings of 2nd Workshop on General Purpose Processing on Graphics Processing Units, ACM, 2009, pp. 79–84.
[13] J. Chan, Z. Wang, A. Modave, J.-F. Remacle, T. Warburton, GPU-accelerated discontinuous Galerkin methods on hybrid meshes, Journal of Computational Physics 318 (2016) 142–168.
[14] G. Cohen, Higher-order Numerical Methods for Transient Wave Equations, Springer-Verlag, 2002.
[15] J. S. Hesthaven, S. Gottlieb, D. Gottlieb, Spectral Methods for Time-dependent Problems, Vol. 21, Cambridge University Press, 2007.
[16] L. V. Kantorovich, V. I. Krylov, Approximate Methods of Higher Analysis, Interscience Publishers, 1958, translated by Curtis D. Benster.
[17] L. Collatz, The Numerical Treatment of Differential Equations, 3rd Edition, Berlin: Springer, 1960.
[18] D. W. Zingg, H. Lomax, H. Jurgens, High-accuracy finite-difference schemes for linear wave propagation, SIAM Journal on Scientific Computing 17 (2) (1996) 328–346.
[19] M. Ghrist, B. Fornberg, T. A. Driscoll, Staggered time integrators for wave equations, SIAM Journal on Numerical Analysis 38 (3) (2000) 718–741.
[20] M. Svärd, J. Nordström, Review of summation-by-parts schemes for initial–boundary-value problems, Journal of Computational Physics 268 (2014) 17–38.
[21] H.-O. Kreiss, N. A. Petersson, J. Yström, Difference approximations for the second order wave equation, SIAM Journal on Numerical Analysis 40 (5) (2002) 1940–1967.
[22] K. Mattsson, J. Nordström, High order finite difference methods for wave propagation in discontinuous media, Journal of Computational Physics 220 (1) (2006) 249–269.
[23] W. D. Henshaw, A high-order accurate parallel solver for maxwell's equations on overlapping grids, SIAM Journal on Scientific Computing 28 (5) (2006) 1730–1765.
[24] E. Hairer, C. Lubich, G. Wanner, Geometric Numerical Integration: Structure-preserving Algorithms for Ordinary Differential Equations, Vol. 31, Springer Science & Business Media, 2006.
[25] R. Warming, B. Hyett, The modified equation approach to the stability and accuracy analysis of finite-difference methods, Journal of Computational Physics 14 (2) (1974) 159–179.
[26] M. A. Dablain, The application of high-order differencing to the scalar wave equation, Geophysics 51 (1) (1986) 54–66.
[27] G. Cohen, Fourth-order schemes for the 2-D wave equation in a homogeneous medium, in: 1986 SEG Annual Meeting, 1986.

[28] G. Shubin, J. Bell, A modified equation approach to constructing fourth order methods for acoustic wave propagation, SIAM Journal on Scientific and Statistical Computing 8 (2) (1987) 135–151.
[29] G. Cohen, P. Joly, Construction analysis of fourth-order finite difference schemes for the acoustic wave equation in nonhomogeneous media, SIAM Journal on Numerical Analysis 33 (4) (1996) 1266–1302.
[30] J. Tuomela, On the construction of arbitrary order schemes for the many dimensional wave equation, BIT Numerical Mathematics 36 (1) (1996) 158–165.
[31] L. Anné, P. Joly, Q. H. Tran, Construction and analysis of higher order finite difference schemes for the 1D wave equation, Computational Geosciences 4 (3) (2000) 207–249.
[32] P. Joly, J. Rodríguez, Optimized higher order time discretization of second order hyperbolic problems: Construction and numerical study, Journal of Computational and Applied Mathematics 234 (6) (2010) 1953–1961.
[33] J. W. Banks, W. D. Henshaw, Upwind schemes for the wave equation in second-order form, Journal of Computational Physics 231 (17) (2012) 5854–5889.
[34] J. Chabassier, S. Imperiale, Introduction and study of fourth order theta schemes for linear wave equations, Journal of Computational and Applied Mathematics 245 (2013) 194–212.
[35] C. Agut, J. Diaz, A. Ezziani, High-order schemes combining the modified equation approach and discontinuous Galerkin approximations for the wave equation, Communications in Computational Physics 11 (2) (2012) 691–708.
[36] W. F. Spotz, G. F. Carey, A high-order compact formulation for the 3D Poisson equation, Numerical Methods for Partial Differential Equations 12 (2) (1996) 235–243.
[37] A. Kumar, Isotropic finite-differences, Journal of Computational Physics 201 (1) (2004) 109–118.
[38] S. Thampi, S. Ansumali, R. Adhikari, S. Succi, Isotropic discrete Laplacian operators from lattice hydrodynamics, Journal of Computational Physics.
[39] M. Patra, M. Karttunen, Stencils with isotropic discretization error for differential operators, Numerical Methods for Partial Differential Equations 22 (4) (2006) 936–953.
[40] L. Savioja, V. Välimäki, Interpolated rectangular 3-D digital waveguide mesh algorithms with frequency warping, IEEE Transactions on Speech and Audio Processing 11 (6) (2003) 783–790.
[41] C. L. Wagner, J. B. Schneider, An acoustic finite-difference time-domain algorithm with isotropic dispersion, Journal of Computational Acoustics 13 (02) (2005) 365–384.
[42] D. P. Petersen, D. Middleton, Sampling and reconstruction of wave-number-limited functions in N-dimensional Euclidean spaces, Information and Control 5 (4) (1962) 279–323.
[43] Y. Liu, M. K. Sen, A new time–space domain high-order finite-difference method for the acoustic wave equation, Journal of Computational Physics 228 (23) (2009) 8779–8806.
[44] G. D. Smith, Numerical Solution of Partial Differential Equations: with Exercises and Worked Solutions, Oxford University Press, 1965.
[45] W. F. Ames, Numerical Methods for Partial Differential Equations, 2nd Edition, Academic Press, 1977.
[46] R. Renaut-Williamson, Full discretizations of $u_{tt} = u_{xx}$ and rational approximations to $\cosh \mu z$, SIAM Journal on Numerical Analysis 26 (2) (1989) 338–347.
[47] J. Tuomela, A note on high order schemes for the one dimensional wave equation, BIT Numerical Mathematics 35 (3) (1995) 394–405.
[48] G. G. O'Brien, M. A. Hyman, S. Kaplan, A study of the numerical solution of partial differential equations, Journal of Mathematical Physics 29 (1950) 223–251.
[49] L. N. Trefethen, Group velocity in finite difference schemes, SIAM Review 24 (2) (1982) 113–136.
[50] G. Cohen, P. Joly, Description and analysis of schemes, fourth-order in time and space, for 1-D and 2-D acoustic equations, in: Society of Exploration Geophysicists Annual Meeting, 1987.
[51] B. Hamilton, S. Bilbao, Fourth-order and optimised finite difference schemes for the 2-D wave equation, in: Proceedings of the International Conference on Digital Audio Effects (DAFx), Maynooth, Ireland, 2013, pp. 146–153.
[52] S. Bilbao, Parameterized families of finite difference schemes for the wave equation, Numerical Methods for Partial Differential Equations 20 (3) (2004) 463–480.
[53] J. Tuomela, Fourth-order schemes for the wave equation, Maxwell equations, and linearized elastodynamic equations, Numerical Methods for Partial Differential Equations 10 (1) (1994) 33–63.
[54] B. Hamilton, S. Bilbao, FDTD methods for 3-D room acoustics simulation with high-order accuracy in space and time, IEEE/ACM Transactions on Audio, Speech, and Language Processing 25 (11) (2017) 2112–2124.
[55] R. P. Muñoz, M. Hornikx, Hybrid Fourier pseudospectral/discontinuous Galerkin time-domain method for wave propagation, Journal of Computational Physics.
[56] T. H. Duong, P. Joly, A principle of images for absorbing boundary conditions, Numerical Methods for Partial Differential Equations 10 (4) (1994) 411–434.
[57] M. Almquist, I. Karasalo, K. Mattsson, Atmospheric sound propagation over large-scale irregular terrain, Journal of Scientific Computing 61 (2) (2014) 369–397.
[58] S. Bilbao, Numerical Sound Synthesis: Finite Difference Schemes and Simulation in Musical Acoustics, John Wiley and Sons, Chichester, UK, 2009.
[59] M. Marshall, Positive Polynomials and Sums of Squares, Mathematical Surveys and Monographs, 2008.